Therefore it is concluded that any hydrothermal alteration rarely occured in the dacite (Dc).

3-5-5 Residual Content of Plagioclase

Plagioclase is the most soluble mineral in due courses of hydrothermal alteration, therefore to determine residual content of plagioclase is a useful tool for alteration survey. Fig. 3-5 shows the result of such survey in the El Bramador district. Samples detected some remained plagioclase by a X-ray determination survey are correlated with the V zone of the alteration zoning.

Ore deposits in the El Bramador are located in a zone, where plagioclase entirely disappeared, and no ore deposit is located in a zone of remained plagioclase. It is indicated that areas involved ore deposits in the La Concha and El Bramador districts are subjected to strong alteration. This fact is similar to Japanese Cenozoic Kuroko situation. Therefore it is said that perfect decomposition zones of plagioclase are potential areas for Kuroko ores. However some remained plagioclase is noted in outskirts zone of Kuroko ores in some cases. In any cases further detailed survey for that is required.

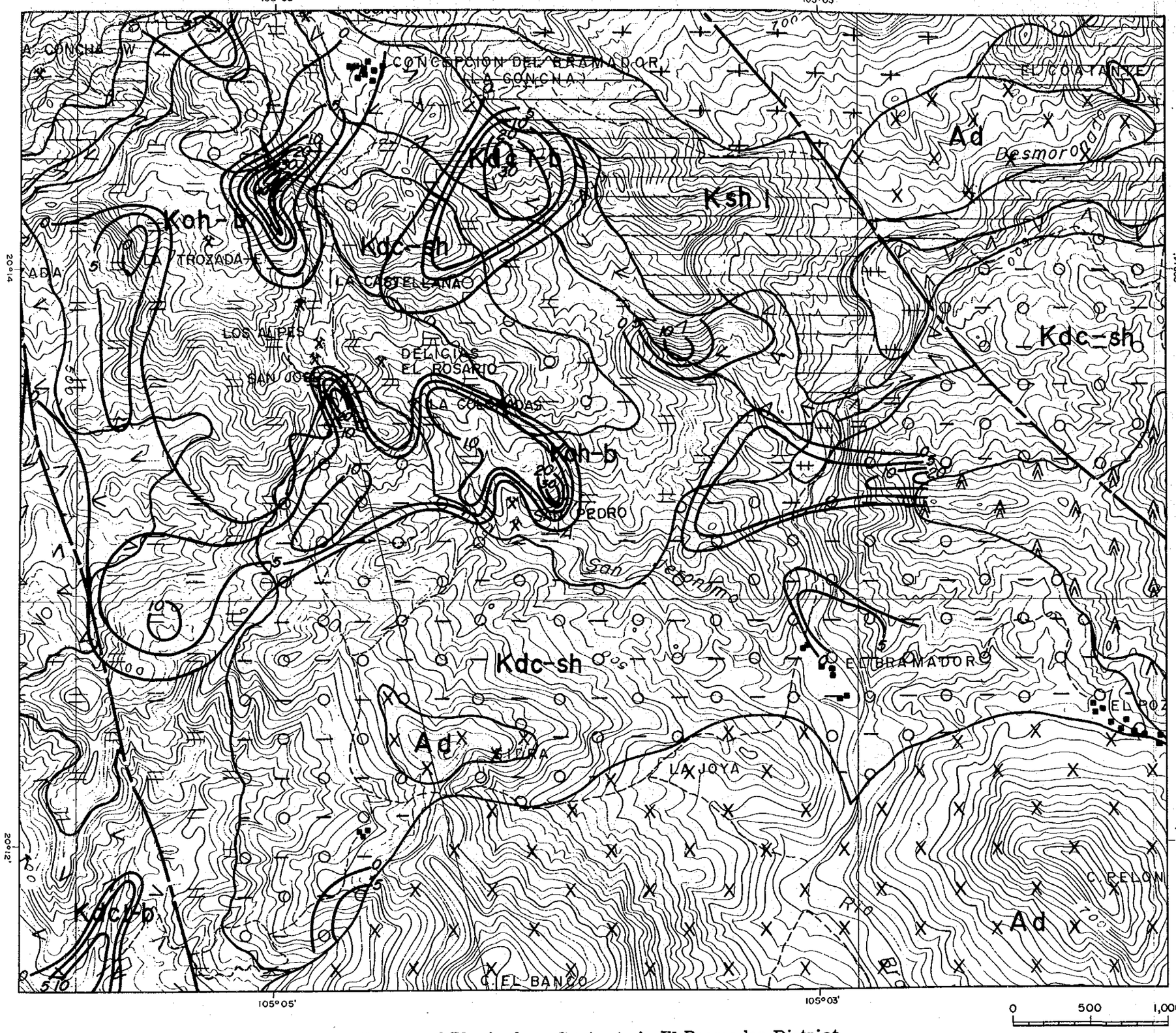

LEGEND

Tertiary System

- Tdc l — I-Stage Dacite-Pyroclastics

Cretaceous System

- Kdc-sh — Hanging Wall Dacite-Pyroclastics-Shale
- Koh-a — Ore Horizon Pyroclastics
- Kdcl-a — Footwall Dacite
- Ksh l — Shale Intercalated with Sandstone

Jurassic System

- Jsch — Metamorphic Rocks

Intrusives

- Dc — Dacite
- Gph — Granophyre
- Ad — Andesite
- Gd — Granodiorite

- Fault
- Contours of Plagioclase Contents by Quartz Index

Fig. 3-5 Distribution of Plagioclase Contents in El Bramador District

CHAPTER 4 GEOCHEMICAL EXPLORATION

CHAPTER 4 GEOCHEMICAL EXPLORATION

4-1 Geochemical Exploration using Stream Sediments

4-1-1 Method of Survey

(1) Sample Collection

In the geochemical exploration using stream sediments, samples were collected checking sample collecting points, which were established previously so as to cover the entire survey area, on topographical maps and with barometers. In a survey area of 1,000 km^2, 1,012 samples were collected. Sample collecting places were on the bank of a stream, the sandbank in a stream or in the underneath of a rock, etc., and a sample of about 30 g of -80 mesh size was collected in each place. The analytical results of these samples are shown in Apx. 1 together with the geology which determines the origin of each sample, collected position, etc.

(2) Preparation of Sample and Detection Limit of Analysis

The samples were dried at the survey base (Talpa de Allende), magnetite was removed from them with magnets, about a quantity of 20 g was separated from each sample for analysis, and after preparing sample lists, the samples for analysis were sent to Hanaoka Laboratory of Dowa Mining Co., Ltd.

Analytical detection limits were all 0.1 ppm for Ag, Cu, Pb and Zn. As the frequency of appearance of values below the detection limit was high (80%) for Ag, statistical treatment was carried out by assuming the values below the detection limit as 0.01 ppm.

4-1-2 Statistical Treatment of Analytical Values

Single variable and multivariable analyses were carried out for the four elements (Ag, Cu, Pb and Zn) of 1,012 samples collected during this survey. In geochemical data analyses, it has been known empirically that the frequency distribution of the contents of minor elements contained in geochemical samples assumes log normal distribution (Lepeltier, 1969). Accordingly, it has been the general method of determining anomalous values to pay attention to the deviation (anomalous population) from the log normal distribution (background population) shown by the most part of a certain indicator. The population handled in geochemical exploration is usually the composite population of the background population and the anomalous population, and it becomes an important subject how to divide these two in conformity with actual conditions. Apart from the case where the object composite population assumes log normal distribution, when the population assumes a distribution deviated from the log normal distribution, particular consideration is required. In the past, a method to determine background values and threshold values using a cumulative frequency distribution curve by Lepeltier (1969) and Sinclair (1976) has been used as a method to solve this problem.

However, a composite population shown by actual geochemical data is usually an assembly of several kinds of populations each having different geochemical characteristics. Therefore, there is a problem in the manner to divide a composite

population into each element population at the bending points on the cumulative frequency distribution curve or at the middle points of curves which appear near the boundaries of plural different populations. As we thought is rational to use the method to determine a frequency curve by determining a spline function approximate to the cumulative frequency curve and its derivative of the first order, which was recently devised by Otsu et al. (1983), to solve the above problem, we used this method for determining the threshold values of single variables. However, to a case where the cumulative frequency curve or histogram agrees well with the log normal distribution curve, the meaning to apply the method by Otsu et al. becomes less, because the population in this case is regarded to be composed of a single population. However, in this survey, it was possible to detect some abnormal population for each of the four elements.

4-1-3 Background Geology and Indicator Content

The contents of indicators in the stream sediments depend upon the geological conditions and the degrees of mineralization and alteration of the background area from which the sediments came from. Accordingly, geochemical characteristics for respective geological units are shown in Table 4-1. However, as the number of samples included in each geological unit was small, threshold values were not determined. According to this table, geological units which have background areas with clearly higher geometric means than that of the entire area are as follows.

Ag : Dacites of the Cretaceous System (Kdc1-a, -b; Koh-a, -b; Kdc-sh)

Cu : I-stage andesites (Tad_1)

Pb : Dacites of the Cretaceous System (Kdc1-a, -b; Koh-a, -b; Kdc-sh)

Zn : Dacites of the Cretaceous System (Kdc1-a, -b; Koh-a, -b; Kdc-sh)

4-1-4 Determination of Threshold Values

Threshold values were determined by smoothing a cumulative frequency curve, drawing a frequency distribution curve, which was determined from the differential coefficients of the smoothed curve, using a spline function, and extracting high content peaks for principal peaks.

Ag: As 80% samples showed values below the detection limit[1)], samples were divided into a non-detected group and a detected group. As the Ag contents of the detected group samples are generally low, the distribution of this group is represented as a stepped cumulative frequency curve in relation to the accuracy of the analysis.

In frequency distribution is clearly different from the low content part with 1.2 ppm as a boundary. Therefore, 1.2 ppm was determined as a threshold value for dividing background values and anomalous values. About 5.4 percent of the whole belongs to the anomalous value.

---

1) To carry out principal component analysis, values below the detection were handled as 0:01 ppm in statistical treatment.

Table 4-1 Statistical Parameters of Geochemical Indicators

Rock Code	Number of Samples	Geometric Mean(ppm)				Threshold (ppm)				Minium Value (ppm)				Maximum Value(ppm)				Standard Deviation (Log)			
		Ag	Cu	Pb	Zn	Ag	Cu	Pb	Zn	Ag	Cu	Pb	Zn	Ag	Cu	Pb	Zn	Ag	Cu	Pb	Zn
Whole Rocks	1,012	0.02	12.3	25.8	68.9	1.2	136	147	440	<0.1	<0.1	<0.1	3.0	86.2	861.0	936.0	979.2	0.74	0.53	0.53	0.35
0	197	0.02	16.4	27.7	87.0	—	—	—	—	<0.1	1.5	<0.1	9.9	53.8	419.2	747.8	941.0	0.77	0.32	0.37	0.37
1	142	0.07	20.8	46.2	111.9	—	—	—	—	<0.1	0.7	0.1	6.4	86.2	516.8	936.0	979.2	0.11	0.51	0.46	0.42
2	69	0.01	43.8	33.5	76.5	—	—	—	—	<0.1	4.6	13.3	24.9	0.3	121.1	68.2	122.4	0.31	0.34	0.15	0.13
3	4	0.02	40.0	31.6	62.4	—	—	—	—	<0.1	28.3	27.5	48.9	0.2	69.9	40.1	87.8	0.65	0.17	0.08	0.11
4	123	0.02	17.4	31.5	68.5	—	—	—	—	<0.1	1.6	<0.1	15.5	23.8	244.6	535.3	303.9	0.52	0.48	0.41	0.21
5	61	0.01	8.8	17.8	54.4	—	—	—	—	<0.1	<0.1	<0.1	15.5	0.2	77.4	61.2	107.8	0.38	0.57	0.87	0.20
6	1	—	—	—	—	—	—	—	—	—	—	—	—	1.6	31.2	309.8	293.7	—	—	—	—
7	367	0.02	6.1	17.9	50.5	—	—	—	—	<0.1	0.7	<0.1	3.0	71.8	861.0	754.0	948.0	0.61	0.44	0.60	0.35
8	48	0.02	15.3	34.0	79.3	—	—	—	—	<0.1	0.9	11.2	33.5	7.7	115.4	677.0	894.0	0.70	0.69	0.28	0.23
11	109	0.09	19.3	50.8	121.4	—	—	—	—	<0.1	2.3	9.5	6.4	86.2	516.8	936.0	979.2	0.12	0.52	0.49	0.44
12	33	0.03	26.8	33.7	85.5	—	—	—	—	<0.1	0.7	9.9	11.7	22.4	159.5	274.0	367.0	0.80	0.47	0.29	0.33

Rock Code

0 : Metamorphic Rocks (Jsch)

1 : Cretaceous System (= Rock Code 11 + 12)

2 : I — Stage Andesites (Tad_1)

3 : Sandstone (Tss_1)

4 : II — Stage Andesites (Tad_2)

5 : III ~ IV — Stage Andesites (Tad_3, Tad_4)

6 : I — Stage Dacites (Tdc_1)

7 : Intrusives (Gd, Gph)

8 : Others (Q, Dc, etc.)

11 : Dacites in Cretaceous System ($Kdc_1^{-b}_{a}$, Kdc-sh, Koh^{-b}_{a})

12 : Shale (Sandstone) in Cretaceous System (Ksh_1)

Fig. 4-1 Frequency and Cumulative Frequency Curve (I)

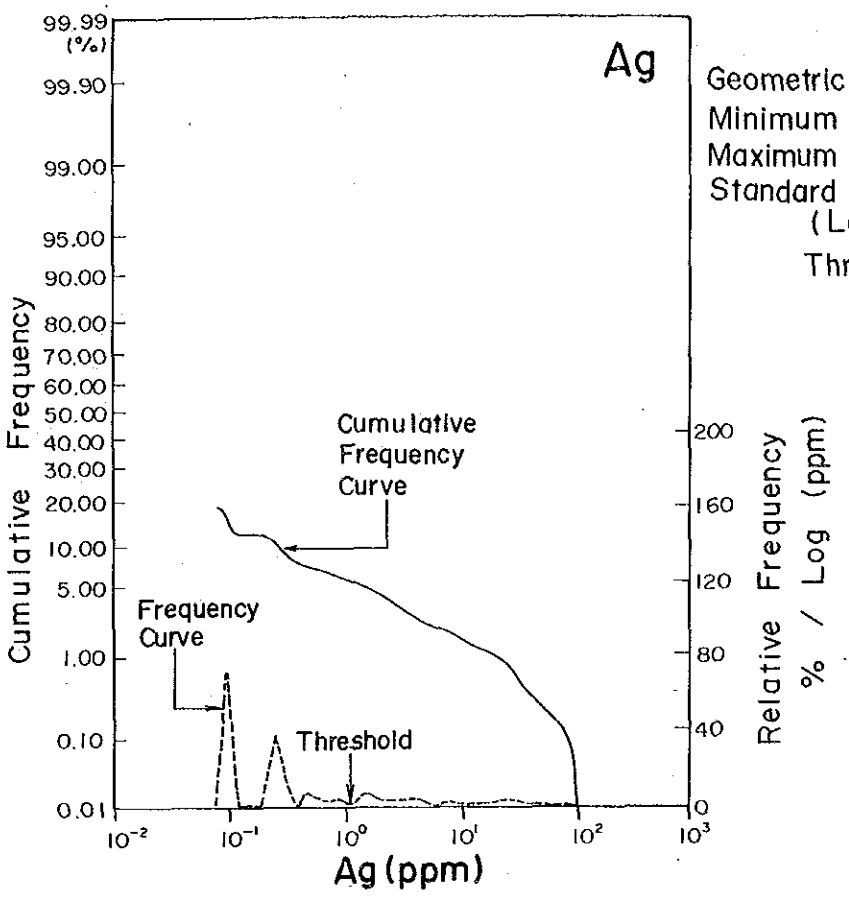

N	: 1012
Geometric Mean	: 0.02ppm
Minimum Value	: <0.1 ppm
Maximum Value	: 86.2ppm
Standard Deviation (Log)	: 0.74
Threshold	: 1.2ppm

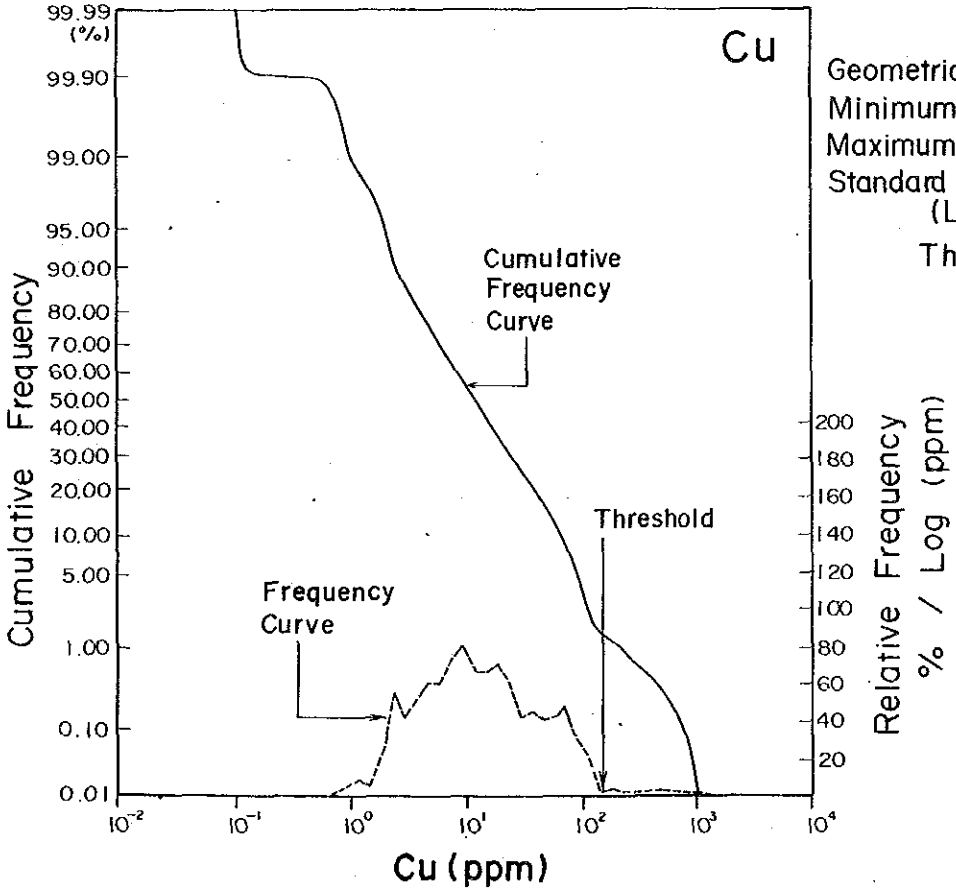

N	: 1012
Geometric Mean	: 12.3 ppm
Minimum Value	: <0.1 ppm
Maximum Value	: 861.0ppm
Standard Deviation (Log)	: 0.52
Threshold	: 136ppm

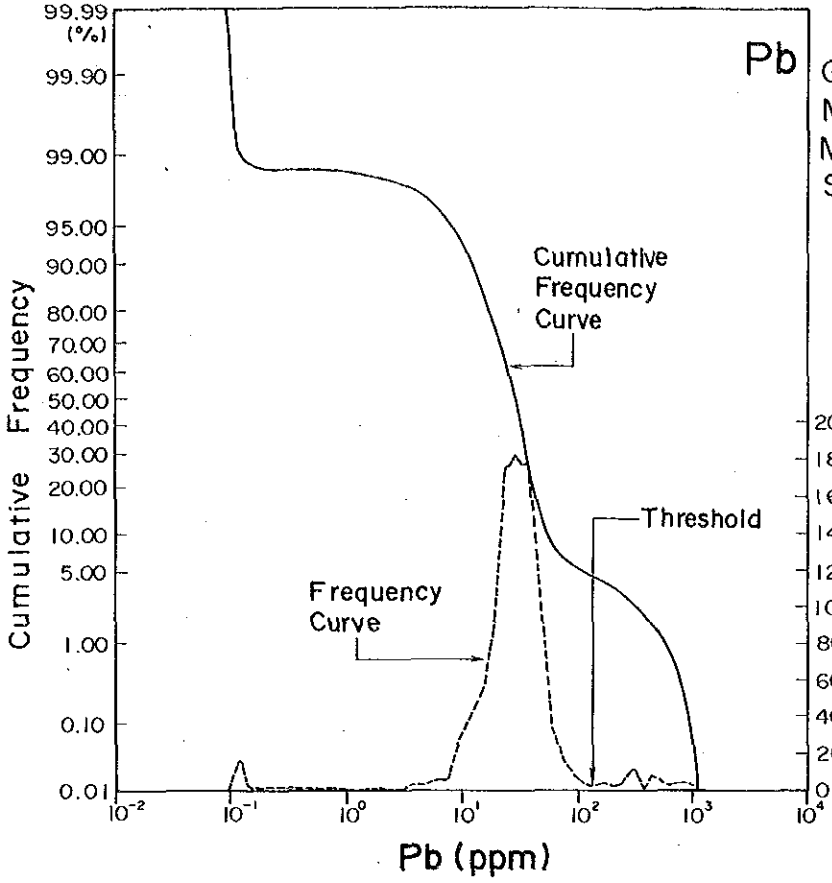

N : 1012
Geometric Mean : 25.8ppm
Minimum Value : <0.1 ppm
Maximum Value : 936.0ppm
Standard Deviation (Log) : 0.53
Threshold : 147ppm

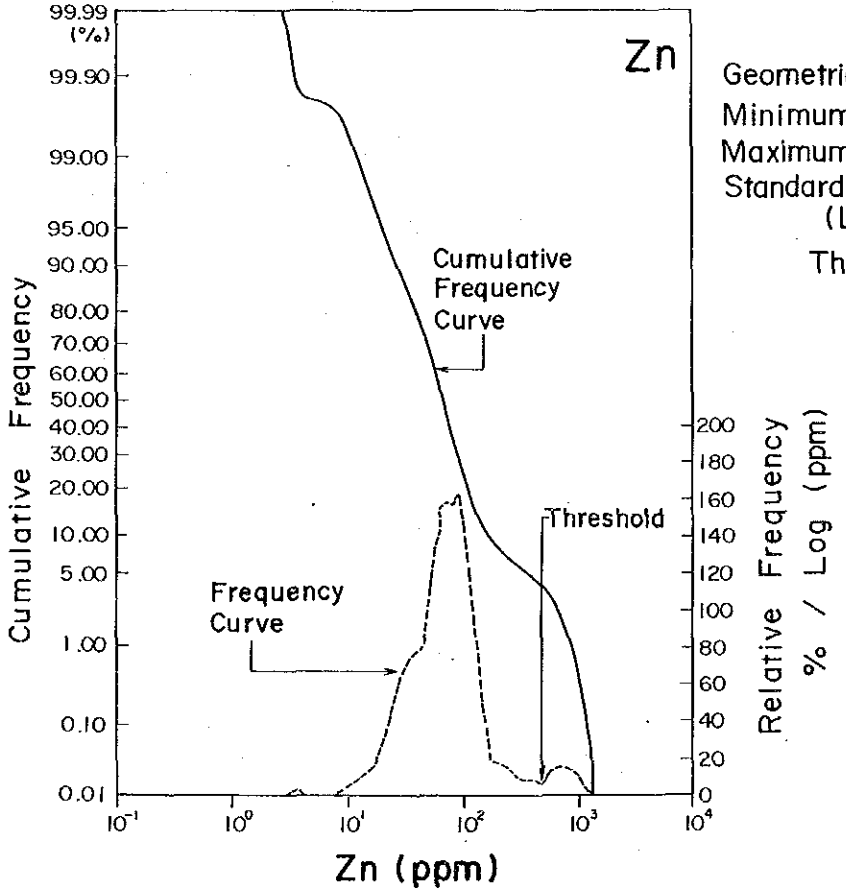

N : 1012
Geometric Mean : 68.9ppm
Minimum Value : 3.0ppm
Maximum Value : 979.2ppm
Standard Deviation (Log) : 0.35
Threshold : 440ppm

Fig. 4-2 Scatter Diagram of Cretaceous System (Cu-Zn), (Pb-Zn)

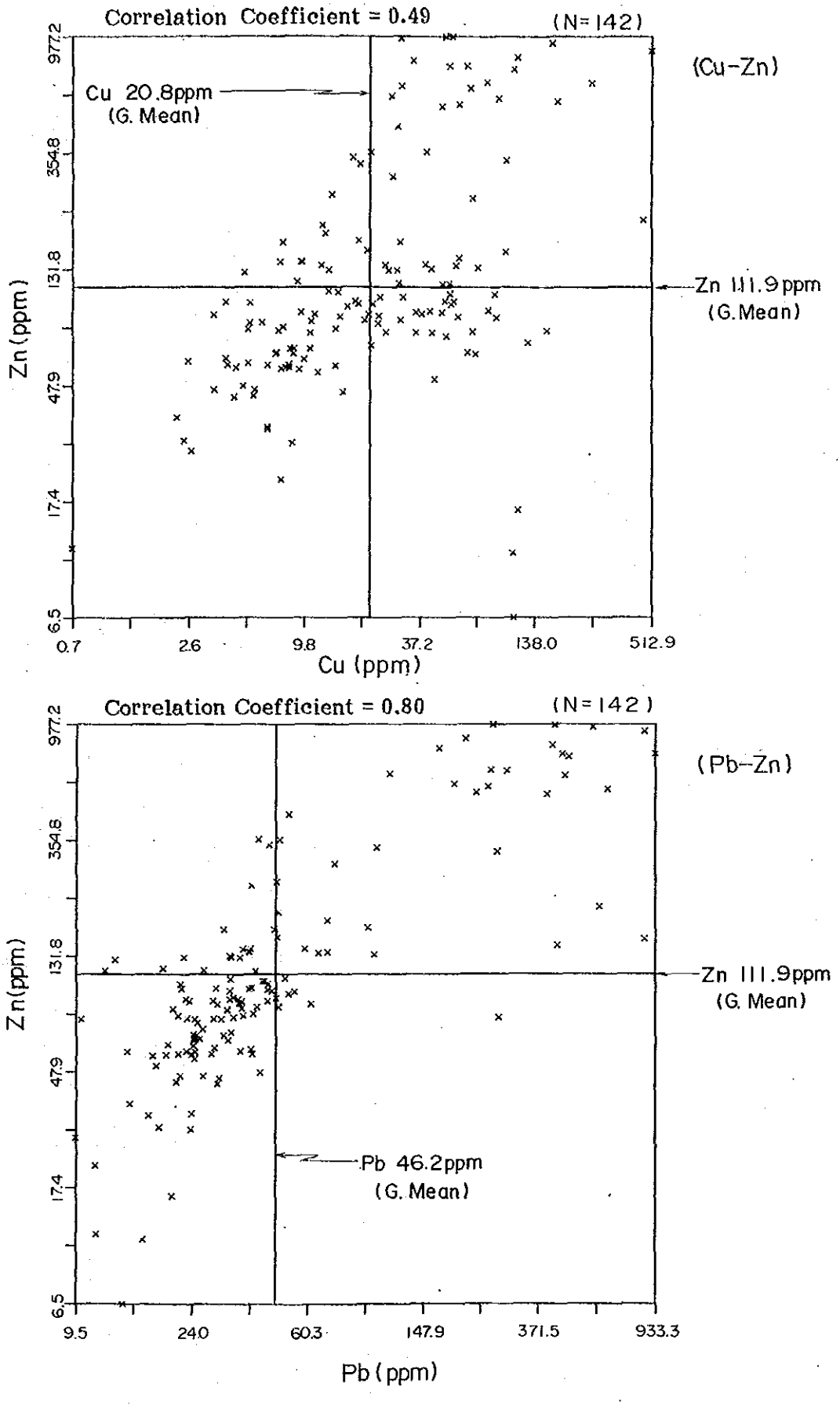

Table 4-2 Matrix of Correlation Coefficient (4 Elements)

(Jurassic System: Jsch) N = 197

R.C. 0

	Ag	Cu	Pb	Zn
Ag	1.00			
Cu	** 0.53	1.00		
Pb	** 0.52	** 0.45	1.00	
Zn	** 0.65	** 0.71	** 0.54	1.00

*: r(0.05) = 0.14, **: r(0.01) = 0.18

(Cretaceous System) N = 142

R.C. 1

	Ag	Cu	Pb	Zn
Ag	1.00			
Cu	** 0.46	1.00		
Pb	** 0.76	** 0.57	1.00	
Zn	** 0.67	** 0.49	** 0.80	1.00

*: r(0.05) = 0.16, **: r(0.01) = 0.21

(I-Stage Andesites: Tad_1) N = 69

R.C. 2

	Ag	Cu	Pb	Zn
Ag	1.00			
Cu	-0.19	1.00		
Pu	0.07	* 0.27	1.00	
Zn	0.07	** 0.32	** 0.55	1.00

*: r(0.05) = 0.27, **: r(0.01) = 0.31

(Sandstone: Tss_1) N = 4

R.C. 3

	Ag	Cu	Pb	Zn
Ag	1.00			
Cu	* 0.96	1.00		
Pb	0.15	0.32	1.00	
Zn	0.86	0.88	0.61	1.00

*: r(0.05) = 0.95, **: r(0.01) = 0.99

(II-Stage Andesites: Tad_2) N = 123

R.C. 4

	Ag	Cu	Pb	Zn
Ag	1.00			
Cu	* 0.19	1.00		
Pb	** 0.25	* 0.20	1.00	
Zn	** 0.24	** 0.36	** 0.46	1.00

*: r(0.05) = 0.18, **: r(0.01) = 0.23

(III - IV-Stage Andesites: Tad_{3-4}) N = 61

R.C. 5

	Ag	Cu	Pb	Zn
Ag	1.00			
Cu	-0.04	1.00		
Pb	* -0.27	0.04	1.00	
Zn	0.15	** 0.41	0.24	1.00

*: r(0.05) = 0.25, **: r(0.01) = 0.33

(Intrusives: Gd, Gph) N = 367

R.C. 7

	Ag	Cu	Pb	Zn
Ag	1.00			
Cu	** 0.45	1.00		
Pb	** 0.29	** 0.34	1.00	
Zn	** 0.58	** 0.58	** 0.38	1.00

*: r(0.05) = 0.10, **: r(0.01) = 0.13

(Others: Q, Dc, etc.) N = 48

R.C. 8

	Ag	Cu	Pb	Zn
Ag	1.00			
Cu	-0.19	1.00		
Pb	** 0.71	0.14	1.00	
Zn	* 0.31	0.25	** 0.49	1.00

*: r(0.05) = 0.28, **: r(0.01) = 0.37

(Dacites in Cretaceous: (Kdc-sh / Kdc1-a, -b, Koh-a, -b) N = 109

R.C. 11

	Ag	Cu	Pb	Zn
Ag	1.00			
Cu	** 0.52	1.00		
Pb	** 0.76	** 0.63	1.00	
Zn	** 0.70	** 0.53	** 0.83	1.00

*: r(0.05) = 0.19, **: r(0.01) = 0.25

(Shale (Sandstone) in Cretaceous: Ksh1) N = 33

R.C. 12

	Ag	Cu	Pb	Zn
Ag	1.00			
Cu	* 0.35	1.00		
Pb	** 0.65	** 0.50	1.00	
Zn	** 0.40	** 0.50	** 0.60	1.00

*: r(0.05) = 0.34, **: r(0.01) = 0.44

Whole Rocks N = 1,012

	Ag	Cu	Pb	Zn
Ag	1.00			
Cu	** 0.36	1.00		
Pb	** 0.39	** 0.38	1.00	
Zn	** 0.59	** 0.54	** 0.49	1.00

*: r(0.05) = 0.06, **: r(0.01) = 0.08

Abbreviation

R.C. : Rock Code

r(0.05) : Significance at the 5% level

r(0.01) : Significance at the 1% level

Cu: In the mode of distribution of the whole rock, the cumulative frequency curve shows negative skewness on the high content side. However, the frequency distribution is clearly different between the low content side and the high content side with 136 ppm as a boundary, so this value was determined as a threshold value. About 1.4 percent of the whole belongs to the anomalous value, showing poor copper-mineralization in the survey area.

Pb: The mode of distribution shows positive skewness on high content side, and small peaks, probably reflecting anomalous value populations, appear on the high content side, bordering at the value of 147 ppm. Therefore this value was adopted as a threshold value. About 4.2 percent of the whole belongs to the anomalous value.

Zn: It shows a distribution with a high degree of concentration as well as Pb. The clear positive skewness is also observed on the high content side. The frequency curve shows clear difference in the distribution mode of populations between the high content side and the low content side with 440 ppm as a boundary. Therefore, 440 ppm was adopted as a threshold value. About 4.2 percent of the whole belong to the anomalous value.

4-1-5 Correlation Coefficient between Indicators

The correlation coefficient between indicators on logarithmic base is shown for the whole rock and each geological unit. In the geological units except the Cretaceous system, correlation coefficients between respective indicators are small, suggesting that the origins of individual indicators are different from each other. However, among the samples originating from the Cretaceous system, especially the combinations of Pb-Zn, Ag-Zn and Ag-Pb of dacites are noticed high correlation coefficient, which is regarded to show that these indicators are those of the same origin, in other words, they are those from the Kuroko type ore are existing in this geological unit.

Using the list of correlation coefficients, tests of 1% and 5% significance levels were carried out (Table 4-2).

4-1-6 Principal Component Analysis

By determining the correlation coefficients between indicators, which cannot be extracted by single variable analyses, from multi-dimensional distribution characteristics, they were applied to the determination of character and the evaluation of geochemical anomalies (Table 4-3).

Table 4-3 Results of Principal Component Analysis

P.C.	Eigen-values	C.R.	Eigenvectors				Factor Loading				Max. Score	Min Score
			Ag	Cu	Pb	Zn	Ag	Cu	Pb	Zn		
Z_1	2.38	0.60	0.49	0.47	0.47	0.57	0.75	0.72	0.73	0.87	6.41	-4.33
Z_2	0.67	0.16	-0.66	0.75	-0.02	-0.04	-0.54	0.62	-0.02	-0.03	1.89	-5.23
Z_3	0.61	0.16	-0.34	-0.28	0.88	-0.21	-0.26	-0.22	0.68	-0.16	1.03	-6.39

Abbreviation
P.C. : Principal Component
C.R. : Contribution Ratio

As shown in this table, the contribution ratio for the first principal component to all the principal components is about 60%, occupying more than a half of all. The total to the ratio of the third principal component amounts to 92% approximately, so that a greater part of the fluctuation of all the components can be explained with them. However, the contribution ratio of the second and the third principal component markedly drop to 16%.

Factor loading is composed of correlation coefficients between principal components and variables (indicator contents). For the first principal component, all indicators show a high value 0.72-0.87. Therefore, the first principal component is characterized by high correlation with all indicators, especially Zn (0.87).

The second principal component is characterized by the high correlation (0.62) with Cu and the negative correlation (-0.54) with Ag. The third principal component has the high correlation with Pb and the low negative correlation with Ag, Cu, and Zn. However, there are few geochemical anomalies with a structure characterized by the third principal component.

4-1-7 Evaluation of Geochemical Anomalies using Stream Sediments

The anomalous zone in the survey area is classified into the single element showing type and the multi-element showing type by a combination of indicators showing the anomaly. In the former case, a comparison and study based upon the contrast of the content of the indicators forming each anomalous zone and the background value of the governing geological unit of the sample, or a comparison and study based upon the first to third factor loading are necessary. Furthermore, the anomalous zone can be classified into several specific zones. The latter multi-element showing type can be classified into two element types among Ag-Pb-Zn and three or more element type among Ag-Cu-Pb-Zn. The explanation and evaluation of each anomaly are as follows:

(1) Single Element Showing Type - Ag

The evaluation list of the anomalous zone is shown in Table 4-4.

This type of anomalous zone has a close relation with the geological unit and is found in intrusive rocks (Gd, Gph), Cretaceous System dacite (Kdc1-a, -b, Koh-a -b, etc.), metamorphic rocks and granodiorite, etc. The type found in metamorphic rocks is found in the El Caracol and La Concha areas. The type found in intrusive rocks (GD, Gph) is found in the San Francisco and Aguacate areas. And the type found in dacites (Kdc1-a, -b), etc. is found in the Amaltea and Grandeza areas.

By comparing and studying the first to third principal component scores ($Z_1 \sim Z_3$) presented by these anomalous zone groups, the geochemical characteristics of each anomalous zone becomes clear. In other words, the structures of the principal component scores presented by the anomalous zones at two places in San Francisco resemble each other closely and can be assumed to have the same kind of mineralization. A similar tendency can be found at three places in the El Caracol area. The anomalous zone in Los Alacranes has a special score structure in the Ag anomalous zone group. In this case, Z_1 shows a positive score near zero and is characterized by a low or somewhat low negative score of $Z_2 \sim Z_3$. From these figures, it can be seen that this anomalous zone has a small content of elements (Cu, Pb, Zn) other than Ag, that is, it can be assumed to have a mineralization of only Ag.

(2) Single Element Showing Type - Cu

The anomalous zone of this type is found in the La Minita area only. The geological unit governing the anomalous zone is II-stage andesites (Tad2), but as

Table 4-4 Evaluation of Anomalous Zones (Single Element Showing Type)

Elements	Anomalous Zones	Sample No.	Rock Code	Contents of Indicaters (ppm)				P.C.A! Scores			Type of Inferred Mineralization
				Ag	Cu	Pb	Zn	Z_1	Z_2	Z_3	
Ag	San Francisco	1738	7	3.9 (229)	9.5 (2)	83.2 (5)	414.1 (8)	3.10	-2.28	-0.59	Ag-Zn
		1746	7	2.7 (159)	13.6 (2)	54.3 (3)	232.5 (3)	2.57	-1.88	-0.76	
	El Caracol	1821	0	1.4 (64)	46.2 (3)	62.3 (2)	147.0 (2)	2.59	-0.84	-0.70	Ag
		1822	0	1.3 (59)	37.3 (2)	58.1 (2)	131.0 (2)	2.37	-0.94	-0.65	
		1824	0	1.8 (82)	66.2 (4)	84.1 (3)	88.0 (1)	2.55	-0.69	-0.48	
	El Aguacate	1828	7	1.7 (100)	33.0 (5)	33.4 (2)	38.0 (1)	1.32	-1.05	-0.76	Ag-(Cu)
	Grandeza	1981	11	1.5 (21)	18.4 (1)	96.4 (2)	167.8 (1)	2.51	-1.46	-0.22	Ag
	La Amaltea	2014	11	5.8 (81)	5.0 (0)	13.0 (0)	127.0 (1)	1.42	-2.34	-1.55	Ag
	Los Alacranes	2138	11	2.8 (39)	6.5 (0)	23.7 (1)	33.4 (0)	0.61	-2.24	-0.69	Ag
	La Concha	2213	0	9.2 (418)	21.0 (1)	35.0 (1)	135.9 (2)	2.54	-2.04	-1.28	Ag
Cu	La Minita	2296	4	< 0.1 (0)	162.1 (9)	40.0 (1)	67.8 (1)	0.94	1.89	-0.13	Cu
Pb	El Bramador	2247	11	1.1 (15)	18.7 (1)	271.1 (6)	324.7 (3)	3.29	-1.38	0.41	Pb-(Ag)
	La Minita	2302	4	0.4 (25)	48.1 (3)	175.0 (6)	204.2 (3)	-1.41	-0.12	-0.05	Pb-(Ag)
Zn	El Aguacate	1688	0	0.6 (27)	29.8 (2)	54.1 (2)	590.0 (7)	3.09	-0.85	-0.89	Zn-(Ag)
		1690	0	0.6 (27)	32.2 (2)	52.4 (2)	450.0 (5)	2.92	-0.79	-0.86	
		1692	0	0.1 (5)	23.0 (1)	25.1 (1)	458.9 (5)	2.01	-0.30	-0.96	
		1817	0	0.1 (5)	25.4 (2)	30.7 (1)	723.7 (8)	2.45	-0.26	-0.95	
	El Caracol	1823	0	0.9 (41)	32.0 (2)	53.6 (2)	745.0 (9)	3.40	-0.98	-1.05	Zn-(Ag)
	Grandeza	1965	0	< 0.1 (0)	27.2 (2)	89.4 (3)	667.0 (8)	2.17	0.65	0.27	Zn
	La Amaltea	2017	12	0.9 (13)	29.9 (1)	113.8 (2)	637.0 (6)	3.55	-1.03	-0.45	Zn-(Ag)
	Desmoronado	2037	7	0.4 (24)	48.7 (8)	138.6 (8)	631.7 (13)	3.58	-0.41	-0.26	Zn-(Cu)-(Pb)
		2042	7	< 0.1 (0)	21.8 (4)	54.7 (3)	497.4 (10)	1.69	0.54	0.05	
	El Encino-N	2092	0	0.7 (32)	18.5 (1)	71.4 (3)	476.6 (5)	2.91	-1.21	-0.55	Zn-(Ag)
	El Portezuero	2259	12	0.2 (3)	28.5 (1)	51.5 (1)	448.4 (4)	2.55	-0.45	-0.62	Zn

Rock Code Numbers are shown in Table 4-1.

Figures in blankets = $\frac{\text{Contents in the specimen}}{\text{Geometric mean of the background rock}}$

the anomalous zone is located to the west of the La Minita deposit and is considered with the extended direction in La Minita deposit, it can be considered as an anomaly in a series of Cu mineralization. This anomalous zone feature has a slightly high Z_2 value in the principal component score structure that shows mineralization of only Cu.

(3) Single Element Showing Type - Pb

This type of anomalous zone is found in a part of La Minita and Bramador areas only. The type in the La Minita area is considered to accompany the mineralization of Cu, Zn to some extent. And the type in the Bramador area resembles the multi-element showing type appearing around the Kuroko type deposit.

(4) Single Element Showing Type - Zn

This type of anomalous zone is found in several places as shown in Table 4-4.

In metamorphic rocks (Jsch), this type is found in the El Aguacate, El Caracol, Grandeza, and El Encino-N areas. In the Cretaceous System shale (sandstone) layer, it is found in the La Amaltea and Camacho areas. In Granodiorite (Gd), it is found in the Desmoronado area. The type found in metamorphic rocks (Jsch) is a slightly higher in the contrast of Ag, but the contrast of Cu and Pb is somewhat low and is considered to show the Ag - Zn mineralization. These are presented clearly in the principal component score structure. In addition, the anomalous zone found in granodiorite (Gd) is large in the contrast of Cu and Pb compared with the others and is considered as the showing type accompanying the Cu - Pb mineralization.

(5) Multi-Element Showing Type - Ag, Cu, Pb, Zn

The evaluation list of the anomalous zone by multi-elements is shown in Table 4-5. The zones are classified into multi-element showing types by combination of three elements Ag, Pb, Zn and by the type of combination of Ag-Pb including Cu and Zn. The anomalous zone of Ag-Pb is found in a part of the Grandeza, Tintilahua, El Bramador and La Minita areas. Various kinds of geology (Table 4-5) are found in the background areas of these anomalous zone groups, but the principal component score structures closely resemble each other. In one place in the Tintilahua area and the Grandeza area, Z_3 shows a negative score and a Pb anomaly in both places is considered to be less strong.

The principal component score structure shown by the anomalous zone group in the prevailing area of the Kuroko type deposit and the structure in other places closely resemble each other, and it was impossible to classify them from this aspect. The anomalous zones due to Ag-Zn are found in the El Aguacate, El Caracol, Mina Cuale and El Corazon areas. Each of them is found in metamorphic rocks (Jsch) and granodiorite (Gd) and seems to have a relation to Ag-Zn vein type mineralization.

Taking the geology in the background area into consideration, it seems there is nothing produced by the Kuroko type mineralization in the anomalous zone. However, in the principal component score, the structure of Mina Cuale

Table 4-5 Evaluation of Anomalous Zones (Multi-Element Showing Type) (1)

Elements	Anomalous Zones	Sample No.	Rock Code	Contents of Indicaters (ppm)				P.C.A' Scores			Type of Inferred Mineralization
				Ag	Cu	Pb	Zn	Z_1	Z_2	Z_3	
Ag-Pb	Grandeza	1846	8	7.7 (321)	115.4 (8)	677.0 (20)	62.0 (1)	3.74	-0.93	0.68	Kuroko
		1881	7	10.6 (624)	122.2 (20)	295.5 (17)	216.0 (4)	4.41	-1.06	-0.31	
	Tintilahua	2225	7	1.5 (88)	37.2 (6)	146.2 (8)	147.3 (3)	2.85	-1.02	-0.05	Ag-Cu-Pb vein
	El Bramador	2238	11	13.0 (181)	99.2 (5)	858.6 (19)	152.0 (1)	4.55	-1.27	0.55	Kuroko
		2351	11	3.7 (51)	58.1 (3)	435.1 (9)	144.0 (1)	3.69	-1.11	0.45	
	La Minita	2298	6	1.6 (1)	31.2 (1)	309.8 (1)	293.7 (1)	3.57	-1.20	0.34	Ag-(Cu)-Pb vein
		2299	4	1.3 (81)	33.6 (2)	379.3 (12)	303.9 (4)	3.65	-1.08	0.50	
Ag-Zn	El Aguacate	1815	7	1.4 (82)	23.2 (4)	39.4 (2)	823.0 (16)	3.35	-1.35	-1.31	Ag-Zn vein
		1816	0	5.0 (227)	48.0 (3)	101.6 (4)	560.0 (6)	4.09	-1.38	-0.95	
		1819	0	1.5 (68)	44.3 (3)	44.9 (2)	941.0 (11)	3.77	-0.98	-1.41	
		1829	7	3.9 (229)	74.2 (12)	84.9 (5)	948.0 (19)	4.49	-1.04	-1.27	
	El Caracol	1827	0	2.1 (95)	73.8 (5)	86.0 (3)	669.0 (8)	4.07	-0.79	-1.04	Ag-Zn vein
	Mina Cuale	1856	7	1.4 (82)	39.6 (6)	163.0 (9)	578.4 (11)	3.86	-1.02	-0.33	Ag-Zn vein
	El Corazon	1959	0	10.0 (455)	75.4 (5)	118.0 (4)	498.0 (6)	4.44	-1.37	-1.06	Ag-Zn vein
Pb-Zn	La Amaltea	2013	11	0.5 (7)	48.0 (2)	401.1 (9)	534.6 (5)	3.93	-0.52	0.50	Kuroko
		2015	11	0.5 (7)	34.3 (2)	169.4 (4)	795.1 (7)	3.75	-0.73	-0.14	
Ag-Cu-Pb	Grandeza	1848	11	42.1 (585)	472.7 (23)	607.0 (13)	201.0 (2)	5.56	-0.76	-0.36	Kuroko
	Mina Cuale	1854	7	71.8 (4224)	861.0 (141)	671.0 (37)	212.0 (4)	6.02	-0.60	-0.55	Ag-Cu-Pb vein
	La Amaltea	2003	7	3.4 (200)	329.9 (54)	696.6 (39)	213.0 (4)	4.79	-0.02	0.31	Kuroko
	El Portezuelo	2256	12	22.4 (311)	159.5 (8)	274.0 (6)	77.0 (1)	3.98	-1.13	-0.31	Ag-Cu-Pb vein
	El Banco	2364	4	23.8 (1488)	244.6 (14)	535.3 (17)	69.0 (1)	4.34	-0.90	0.09	Ag-Cu-Pb vein
Ag-Pb-Zn	Mina Cuale	1845	11	1.9 (26)	26.7 (1)	191.3 (4)	583.6 (5)	3.86	-1.39	-0.18	Kuroko
		1847	11	7.0 (97)	54.1 (3)	425.6 (9)	976.0 (9)	5.18	-1.49	-0.16	

Rock Code Numbers are shown in Table 4-1.

Figures in blankets = $\frac{\text{Contents in the specimen}}{\text{Geometric mean of the background rock}}$

Elements	Anomalous Zones	Sample No.	Rock Code	Contents of Indicaters (ppm)				P.C.A' Scores			Type of Inferred Mineralization
				Ag	Cu	Pb	Zn	Z_1	Z_2	Z_3	
Ag-Pb-Zn	Grandeza	1878	11	2.0 (28)	91.8 (4)	251.3 (5)	571.0 (5)	4.44	-0.64	-0.27	Kuroko
		1879	7	2.6 (153)	120.6 (20)	291.0 (16)	704.0 (14)	4.83	-0.59	-0.34	
		1880	11	21.8 (303)	109.1 (5)	476.4 (10)	740.1 (7)	5.62	-1.48	-0.40	
		1885	11	18.3 (254)	52.4 (3)	453.8 (10)	756.4 (7)	5.28	-1.87	-0.24	
		1977	0	25.3 (1150)	124.4 (8)	490.9 (18)	677.0 (8)	5.67	-1.45	-0.41	
		1978	11	1.6 (22)	58.5 (3)	228.3 (5)	543.4 (5)	4.13	-0.83	-0.19	
	El Corazon	1953	8	4.0 (167)	70.2 (5)	301.8 (9)	894.0 (11)	4.92	-1.10	-0.34	Ag-Pb-Zn vein
		1958	0	3.7 (168)	62.5 (4)	268.6 (10)	761.4 (9)	4.70	-1.14	-0.34	
	La Trozada	2220	0	3.2 (145)	43.8 (3)	211.6 (8)	825.5 (9)	4.48	-1.30	-0.42	Ag-Pb-Zn vein
		2221	0	2.1 (95)	39.6 (2)	193.3 (7)	557.0 (6)	4.01	-1.18	-0.27	
	El Bramador	2223	11	4.3 (60)	49.9 (4)	260.7 (6)	979.2 (9)	4.82	-1.35	-0.40	Kuroko
		2239	11	12.2 (169)	66.4 (3)	461.8 (10)	626.9 (6)	5.14	-1.56	-0.15	
		2240	11	6.9 (96)	114.2 (5)	419.2 (9)	819.6 (7)	5.33	-1.01	-0.30	
		2244	11	1.9 (26)	80.1 (4)	256.4 (6)	660.0 (6)	4.49	-0.72	-0.26	
		2245	11	4.8 (67)	63.9 (3)	936.0 (20)	760.4 (7)	5.26	-1.25	0.50	
		2246	11	3.1 (43)	29.7 (1)	576.3 (12)	960.2 (9)	4.82	-1.56	0.36	
Ag-Cu-Pb-Zn	Mina Cuale	1844	11	17.5 (243)	265.1 (13)	290.0 (6)	655.0 (6)	5.63	-0.83	-0.88	Kuroko
		1855	7	32.3 (1900)	696.2 (114)	754.0 (42)	622.0 (12)	6.51	-0.48	-0.53	
	Grandeza	1876	11	25.6 (356)	179.2 (9)	647.2 (14)	558.1 (5)	5.78	-1.23	-0.25	Kuroko
		1877	7	2.4 (141)	278.2 (46)	475.2 (27)	848.0 (17)	5.45	-0.06	-0.21	
	La Amaltea	2005	11	86.2 (1197)	516.8 (25)	210.0 (5)	865.0 (8)	6.41	-1.03	-1.66	Kuroko
		2011	11	30.0 (417)	169.1 (8)	859.3 (19)	924.0 (8)	6.27	-1.35	-0.20	
	El Encino-S	2202	0	53.8 (2445)	419.2 (26)	747.8 (27)	523.0 (6)	6.33	-0.98	-0.48	Ag-Cu-Pb-Zn vein

(Table 4-5) slightly resembles the principal component score structure presented in the prevailing area of the Kuroko type deposit.

The anomalous zone by Pb-Zn is found in the La Amaltea area only and seems to have a close connection with the Kuroko type deposit from the point of view of the geology of the background area and the principal component score structure. In the anomalous zones classified by indicators of more than three elements, the Ag-Cu-Pb, Ag-Pb-Zn and Ag-Cu-Pb-Zn types are found. The Ag-Cu-Pb anomalous zone is found in the Grandeza, Mina Cuale, La Amaltea, El Portezuelo and El Banco areas. Judging from the geology and other factors in the background area, the anomalous zones in the Mine Cuale and La Amaltea areas seem to have a relation to the Kuroko type mineralization, but the anomalous zones in the other areas seem to suggest an anomaly due to vein type mineralization.

However, the principal component score structure in the Amaltea anomalous zone is different from the others. This is due to the fact that the Pb content is relatively high in the sample, and the Cu content is relatively low. The number of Ag-Pb-Zn anomalous zones is the largest among all anomalous zones. They are found in the Mina Cuale, Grandeza, El Bramador, El Corazón, and La Trozada areas. Such anomalous zones have a relation to the geology in the background area, and most of them belong to the dacites and metamorphic rock groups. The anomalous zones in the Mina Cuale and El Bramador areas and most of them in the Grandeza area belong to the Cretaceous System dacites and seem to have a relation to the Kuroko type mineralization. The anomalous zones in the El Corazon and La Trozada areas are found in metamorphic rocks and are considered to have a relation to the vein type mineralization. The Ag-Cu-Pb-Zn anomalous zones are found in the Mina Cuale, Grandeza, La Amaltea and El Encino zones. Among the above anomalous zones, the one in the El Encino-S area exists in metamorphic rocks and seems to have a relation to the vein type mineralization. The anomalous zones in the other areas can be considered to be anomalies related to the Kuroko type mineralization judging from the locational relation to the known Kuroko type deposit and the geology in the background area. From the stand point of the principal component score structure, a clear difference cannot be found between the structure of an anomalous zone which is considered to be the origin of the Kuroko type mineralization and the score structure of the vein type mineralization.

4-2 Geochemical Exploration by Whole Rock Analysis

From the lithogeochemical point of view, trials to classify rocks into two catergories, Kuroko relating and non-Kuroko relating, were done by several investigators (Sopuck et al., 1980; Dudas, 1983; Hashimoto, 1983). However, no versatile method for Kuroko exploration has been established yet, whether it is of principal or minor elements of rocks. It seems that specific areas need to develop their own specific exploration methods, utilizing their own specific characters.

In this survey, a study on this matter was conducted for the footwall decite (Kdc1), hanging wall dacite (Kdc-sh), and intrusive dacite (Dc).

Following studies were conducted using the results of chemical assay of samples, 13 components for each sample.

(1) Interprtation of correlation coefficient

(2) Alkali alteration index,

(3) Principal component analysis,

(4) Cluster analysis.

A study was carried out on the determination of volcanic rock series of the Cretaceous terrain. For the latter two analyses, the last year's assay data for 102 samples were added to third year's data, because the number of the samples is too small to interprete.

The rocks assayed are generally subjected to hydrothermal alteration, but the most fresh ones were selected for determination of rock series, using

$MgO - FeO^* - (Na_2O + K_2O)$,

$SiO_2 - (FeO^*/MgO)$

$FeO^* - (FeO^*/MgO)$ diagrams,

FeO^* : Total Fe as FeO

As a result of the study, several samples selected are plotted in the calc-alkaline rock series domain. This result accords with the idea, which all Kuroko ores are associated with calc-alkaline rock series (Hutchinson 1973; Lambert & Sato, 1974).

4-2-1 Correlation Coefficient

Based on the assay results of the 34 rock samples, a study on relations between the rocks and Kuroko mineralization was done. Table 4-6 shows correlation coefficients on the 13 components.

Table 4-6 Matrix of Correlation Coefficient (13 Chemical Compositions)

N = 3 4

	SiO_2	TiO_2	Al_2O_3	Fe_2O_3	FeO	MnO	MgO	CaO	Na_2O	K_2O	P_2O_5	LOI	BaO
SiO_2	1.00												
TiO_2	-0.33	1.00											
Al_2O_3	**-0.70	0.22	1.00										
Fe_2O_3	-0.08	-0.12	**-0.51	1.00									
FeO	-0.33	0.06	0.02	-0.06	1.00								
MnO	-0.31	**0.50	0.28	-0.05	0.18	1.00							
MgO	*-0.35	-0.10	0.24	-0.15	**0.56	-0.01	1.00						
CaO	*-0.39	0.31	* 0.35	-0.19	0.14	0.20	0.06	1.00					
Na_2O	-0.15	0.23	* 0.42	*-0.43	-0.15	0.20	-0.15	**0.45	1.00				
K_2O	-0.30	0.34	** 0.45	*-0.35	-0.16	0.15	-0.28	-0.04	0.17	1.00			
P_2O_5	**-0.66	**0.47	* 0.39	-0.00	0.26	*0.39	0.01	**0.70	0.15	0.23	1.00		
LOI	**-0.45	-0.12	0.12	* 0.39	*0.38	-0.08	**0.53	0.00	**-0.52	*-0.42	0.22	1.00	
BaO	0.02	0.19	0.23	-0.34	-0.29	0.08	-0.16	0.20	0.19	** 0.44	0.08	*-0.39	1.00

* : Significance at the 5 % level = 0.34

** : Significance at the 1 % level = 0.44

In this table, positive correlation is noticed in the following combinations.

P_2O_5	-	CaO	(0.70)
MgO	-	FeO	(0.56)
MgO	-	LOI	(0.53)
MnO	-	TiO_2	(0.50)
P_2O_5	-	Al_2O_3	(0.45)
CaO	-	Na_2O	(0.45)
BaO	-	K_2O	(0.44)

Following combinations show negative correlations.

SiO_2	-	Al_2O_3	(-0.70)
SiO_2	-	P_2O_5	(-0.66)
Na_2O	-	LOI	(-0.52)
Fe_2O_3	-	Al_2O_3	(-0.51)
SiO_2	-	LOI	(-0.45)

A study was done on the rocks assayed, being generally subjected to hydrothermal alteration.

In cases of being subjected to hydrothermal alteration CaO and Na_2O tend to be depleted from rocks, on the other hand BaO and K_2O tends to be enriched, especially in cases of alteration related to Kuroko minralization, in other words these two combinations show positive correlations.

A combination of MgO and FeO, which lithogeochemically have similar characteristics, also shows a positive correlation. Between SiO_2 and other component, Al_2O_3, P_2O_5, LOI, etc. negative correlations are noted, suggesting tendency of depleting the latter components during silicification.

4-2-2 Alkali Alteration Index*

Alkali alteration index (AAI) is a device to quantitatively evaluate intensity of alteration from the view point of mobility of alkali and alkaline-earth metals during hydrothermal alteration, devised by Ishikawa et al. (1980).

It significantly contributed to the discovery of a Cenozoic Kuroko ores, Ezuri deposit, in Japan.

In this survey, no map showing such alteration intensity was made because the number of samples is too small.

According to the results of the calculation for each sample, strong alteration zones (AAI higher than 90) are shown in the Chivos de Abajo and Naricero deposits in the Cuale Mine, (CC-11, DA-73, WCUM-12).

However, strong alteration zones are shown in the footwall rocks in the El Bramador deposits, and weak alteration zones (AAI lower than 50) are shown near the San Pedro adit (D-68). No other samples were taken around there, therefore details are not clear yet.

---

* Alkali Alteration Index = $(MgO + K_2O)/(MgO + K_2O + Na_2O + CaO) \times 100$
( ) weight %

Judging from the alteration map (Fig. 3-4) by clay mineral assemblage, the sample (D-68) is in the Zone III (Quartz-Chlorite-(Sericite) zone), therefore it is presumed that the result of AAI of the sample indicates a heterogeneity of alteration.

AAI is a very sensitive device to detect strong alteration zones, therefore it is useful for detailed surveys rather than regional one. (Hashiguchi, et al., 1981).

4-2-3 Principal Component Analysis

After standerizing all assay values, a principal component analysis was conducted. Table 4-7 shows the result.

The maximum eigenvalue is 3.67, a square sum of the first factor loadings, being able to explain about 28 percent of the total.

The second, third, and fourth factors are 17, 14, and 11 percent respectively. Accordingly about 70 percent of the all original data is explained by factors up to fourth.

Factor loadings (correlation coefficients between each factor and variate) is the most important element for the analysis, therefore characters of each factor loading were investigated.

Z_1 is characterized by significant negative correlations between SiO_2 and other components, meaning increasing SiO_2 versus decreasing other components. It means that addition of SiO_2 by cilicification is commonly dominant in the area.
Results of the field survey support this fact too.

Z_2 is characterized by negative correlations between acidic components (SiO_2, Al_2O_3, Na_2O, K_2O, BaO, etc.) and basic components (FeO, MgO, etc.). Accordingly it is said that Z_2 is a representative factor loading for lithogeochemical characters of rocks itself.

Z_3 is characterized by negative correlations between K_2O, and Na_2O and CaO, which are most sensitive components for Kuroko type alteration, it means that they take mutually complementary behaviours, and represent characters of movement of components by hydrothermal alteration.

Fe_2O_3 showing the highest factor loading in Z_3 is a good indication for oxidation-reduction eivironment, but it is difficult to find concrete lithogeochemical relations to other factor loadings.

It appears that Z_4 reflects states of alkali and alkaline-earth metals, which are of high mobility in Kuroko type alteration, meaning negative correlations between Na_2O and CaO (decreasing components), and K_2O and MgO (increasing components).

Accordingly distribution of the third and fourth factors, which appear that alkali and alkaline-earth metals mostly contribute for them, is shown in Fig. 4-3. Especially their relations to their geologic environments were investigated.

Geologic domains and sampling points are as follows:

A. Hanging wall dacite (Kdc2, La America-Descubridora district)

Table 4-7 Analytical Results of Principal Component Analysis

N=136

P.C	E.V.	C.R	Factor Loading													Max. Score	Min. Score
			SiO_2	TiO_2	Al_2O_3	Fe_2O_3	FeO	MnO	MgO	CaO	Na_2O	K_2O	P_2O_5	LOI	BaO		
Z_1	3.67	0.28	-0.66	0.61	0.71	0.02	0.47	0.60	0.48	0.63	0.66	0.40	0.55	0.33	0.37	4.41	-8.75
Z_2	2.15	0.45	-0.05	0.14	-0.40	0.34	0.55	0.10	0.51	0.08	-0.41	-0.68	0.29	0.45	-0.59	5.38	-2.57
Z_3	1.86	0.59	0.41	-0.42	-0.10	-0.65	0.40	0.20	0.38	0.50	0.37	-0.27	-0.47	-0.24	0.00	3.34	-3.16
Z_4	1.40	0.70	0.42	0.38	-0.42	0.21	-0.23	0.48	-0.43	0.40	0.15	-0.23	0.28	-0.26	0.11	3.49	-3.18
Z_5	1.12	0.79	0.14	-0.34	-0.07	0.32	-0.10	0.42	0.04	0.06	-0.20	0.11	-0.34	0.57	0.45	2.49	-3.44
Z_6	0.81	0.85	0.21	0.13	-0.25	-0.20	0.35	0.04	0.17	-0.25	-0.33	0.32	0.25	-0.16	0.37	2.32	-3.90

P.C : Principal components
E.V : Eigenvalue
C.R : Contribution ratio
LOI : Loss on ignition

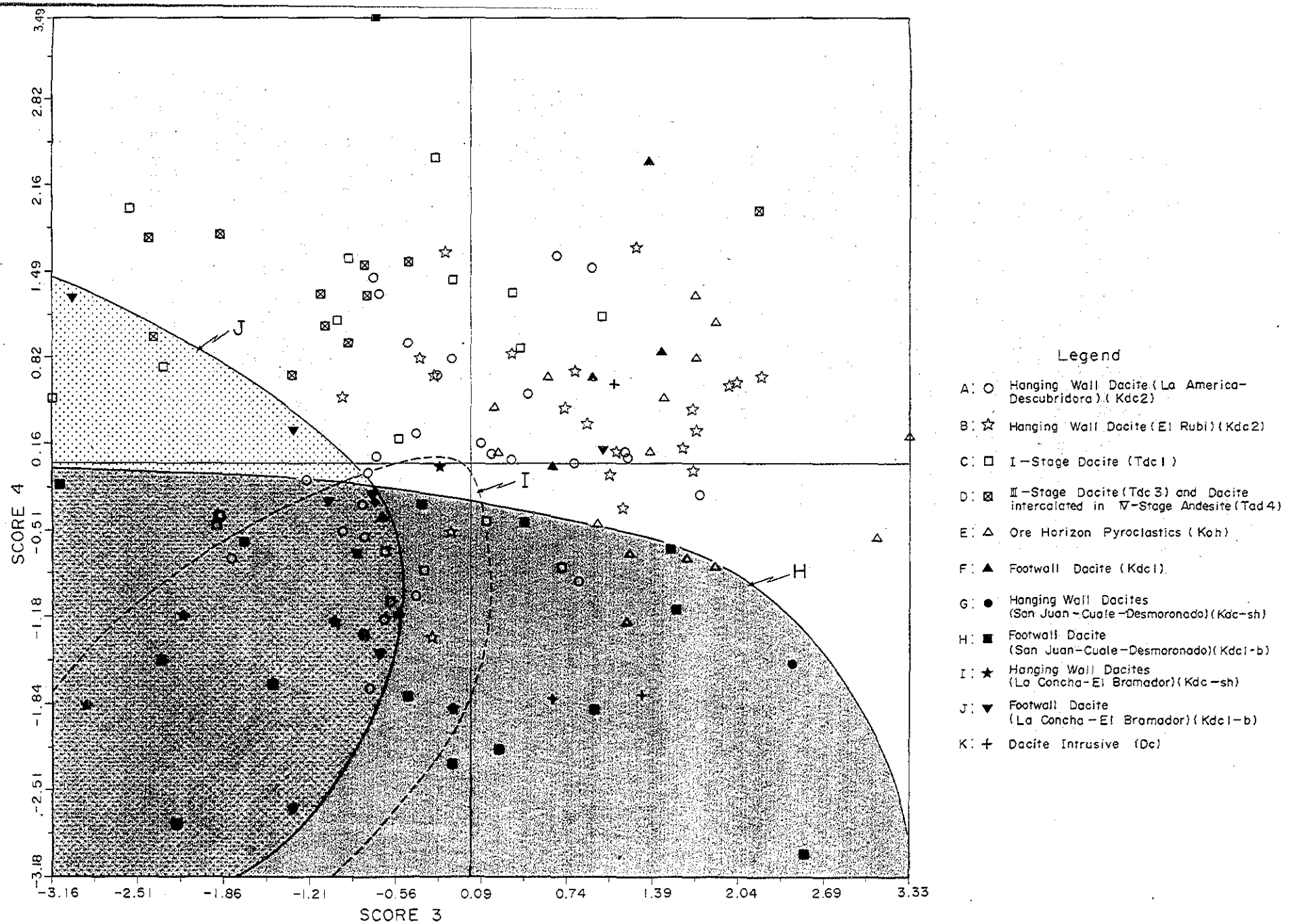

Fig. 4-3 Relation between Factor 3 and Factor 4

B. Hanging wall dacite (Kdc2, El Rubi district)
C. I-stage dacite (Tdc1)
D. III-stage dacite (Tdc3) etc.
E. Ore horizon pyroclastics (Koh)
F. Footwall dacite (Kdc1, La America-Descubridora district)
G. Hanging wall dacite (Kdc-sh, San Juan-Cuale-Desmoronado district)
H. Footwall dacite (Kdc1-b, San Juan-Cuale-Desmoronado district)
I. Hanging wall dacite (Kdc-sh, La Concha-El Bramador district)
J. Footwall dacite (Kdc1-b, La Concha-El Bramador district)
K. Intrusive dacite (Dc, various points)

According to this diagram, the footwall dacite (H group) from the San Juan-Cuale-Desmoronado districts is mostly distributed in the third and fourth quadrants, and is characterized by mostly negative scores in the fourth factor scores.

The footwalll dacites (J group) in the La Concha-El Bramador district is in the second and third quadrants, mostly of negative scores in the third factor scores. J group and H group overlap with each other in the third quadrant, therefore, they have similar geochemical characters.

On the other hand, the scores of the hanging wall dacite (I group) in the La Concha-El Bramador district tend to be distributed in the middle of the previously mentioned two groups.

The H and I groups are extensively distributed, and have no other characteristics than the above mentioned factor scores.

It is due to that even a same rock group shows different factor scores in cases it has different grade of alteration. The hanging wall dacites (G group) in the Cuale district and the intrusive dacite (K group) are lacking in the number of samples and distribnute sparsely on the diagram, therefore details of their lithogeochemical characteristics are not clear.

4-2-4 Cluster Analysis

For the purpose of distinguishing rocks related with Kuroko type ores from those not related or checking for the possibility of dividing each rock group into finer groups, the cluster analysis was carried out using the results of the principal component analysis. The cluster analysis is a method to classify samples into clusters of similar geochemical characteristics in this case based on a certain criterion. The criterion used in this survey is the degree of the nearest neighbor in Euclidean distance from the origin of a six-dimensional space with the six components as axes using the first to the sixth component scores. The results of cluster analysis are shown in Fig. 4-4 in a dendrogram. By this diagram, the relationship between each sample and a cluster can be found. The alphabet before a number shows the geological unit (see previous section) from which the sample originated.

Samples classified into ten categories (A to J) based on their geological domains and sampled points were investigated in view of distribution in each cluster classified in 12 clusters for 136 samples. As a result of the investigation, some characteristics were found in some clusters. Important conclusions from the result are as follows:

Cluster 3; Twenty three samples are involved in the cluster, and main constituents are five out of 16 samples of the footwall dacite (Kdc1-b) in the Cuale-Desmoronado district.

Accordingly it is expected that they are subjected to hydrothermal alteration relating to Kuroko type mineralization.

Comparison between mean chemical compositions for each main cluster is shown in Table 4-8 and Fig. 4-5.

Characteristics of the cluster are comparatively

(1) poor in SiO_2, TiO_2, CaO, Na_2O, K_2O, P_2O_5, and
(2) rich in Al_2O_3, FeO, MgO, LOI, BaO,

to the average components.

Increasing of MgO and K_2O, and decreasing of CaO and MgO are expected in cases of hydrothermal alteration relating to Kuroko type mineralization, however only behaviour of MgO and Na_2O tends to agree to this.

It is judged that the intensity of Kuroko alteration in this group is weak.

Samples involved in this cluster were mainly taken from surrounding zones of Kuroko ores, therefore it is presumed that they show a geochemical characters of the footwall dacite related to Kuroko type ores. A sample from the hanging wall dacite (kdc-sh) in the La Concha-El Bramador district is involved in the cluster.

Fourteen samples from the last year's survey area, six from the ore horizon pyrolastics (Koh) and 8 from the hanging wall dacite (Kdc2) in the La America-Descubridora district, are involved in this cluster.

Cluster 4; Thirtyseven samples are involved in the cluster, which is characterized by involvement of the all intrusive dacite not relating to Kuroko type ores.

Two samples from the footwall dacite (Kdc1-b) in the Cuale and La Concha-El Bramador districts are involved in the cluster.

Sixteen samples from the last year's survey area, eleven from the hanging wall dacite (Kdc2) and five from the I-stage dacite (Tdc1), are involved in the cluster, meaning that this cluster involves rocks not relating to Kuroko type mineralization.

Characteristics of the cluster ore are as follows:

(1) poor in TiO_2, Fe_2O_3, FeO, MnO, MgO, CaO, BaO, LOI, and
(2) rich in SiO_2, Na_2O, K_2O

The rocks involved in this cluster are possibly subjected to silicification judging by the characteristics, however no decreasing of Na_2O, the most sensitive component for hydrothermal alteration, is recognized here.

Accordingly it is judged that rocks of this cluster are subjected to other alteration than of Kuroko type, or very weak alteration. Furthermore alkali alteration indices of the rock samples are generally low.

Cluster 5; Three out of total 15 samples, two from the footwall dacite (Kdc1-b) in the Cuale district and one from the hanging wall dacite (Kdc2-b) in the La Concha-El Bramador district, are involved in the cluster.

Eleven out of 15 samples from the first year's survey year, six from the hanging wall dacite in the La America-Descubridora district and five from the I-stage dacite (Tdc1), are also involved.

Characteristics of the cluster are

(1) poor in TiO_2, FeO, MnO, MgO, CaO, Na_2O, and
(2) rich in SiO_2, K_2O, BaO

This cluster out of seven main clusters shows closer to the mobilization performance of components by hydrothermal alteration related to Kuroko type mineralization. Especially relative decreasing of Na_2O and increaisng of K_2O are very clear.

Furthermore increase of BaO, a principal component of barite, suggests something to Kuroko type mineralization.

However, the degree of relative increase in MgO is insufficient to immediately conclude this cluster as a cluster subjected to the Kuroko type alteration, but this cluster shows characteristics closest to the Kuroko type alteration.

Cluster 6; Four samples, two from the footwall dacite (Kdc1-b) in the Cuale district and one each from hanging wall and footwall dacites (Kdc-sh and Kdc1-b) in the La Concha-El Bramador district, are involved in the cluster.

Characteristics of the cluster are as follows:

(1) poor in SiO_2, TiO_2, Al_2O_3, MgO, CaO, Na_2O, K_2O, BaO, and
(2) rich in Fe_2O_3, LOI

Specially significant increase of Fe_2O_3 and decrease of Na_2O, CaO, and BaO is characteristic.

This performance partly agrees to that of Kuroko type, but reaction of increasing components is not enough to say that of alteration relating to Kuroko ores.

Cluster 8; Five out of total 17 samples, three from the footwall dacite (Kdc1-b) and one from the hanging wall dacites (Kdc-sh) in the La Concha-El Bramador district, and one from the footwall dacites (Kdc2-b) in the Desmoronado district, are involved in the cluster. The samples were taken from far areas from Kuroko ores, being weakly subjected to alteration of Kuroko type.

Characteristics of the cluster are as follows:

(1) poor in SiO_2, BaO, and
(2) rich in TiO_2, Al_2O_3, FeO, Na_2O, P_2O_5

It is much different from that of Kuroko type.

Samples in the last year's survey area, four from the hanging wall dacite (Kdc2) in the La America-Descubridora district and some from the I-stage dacite (Tdc1) of Tertiary system, are involved in the cluster.

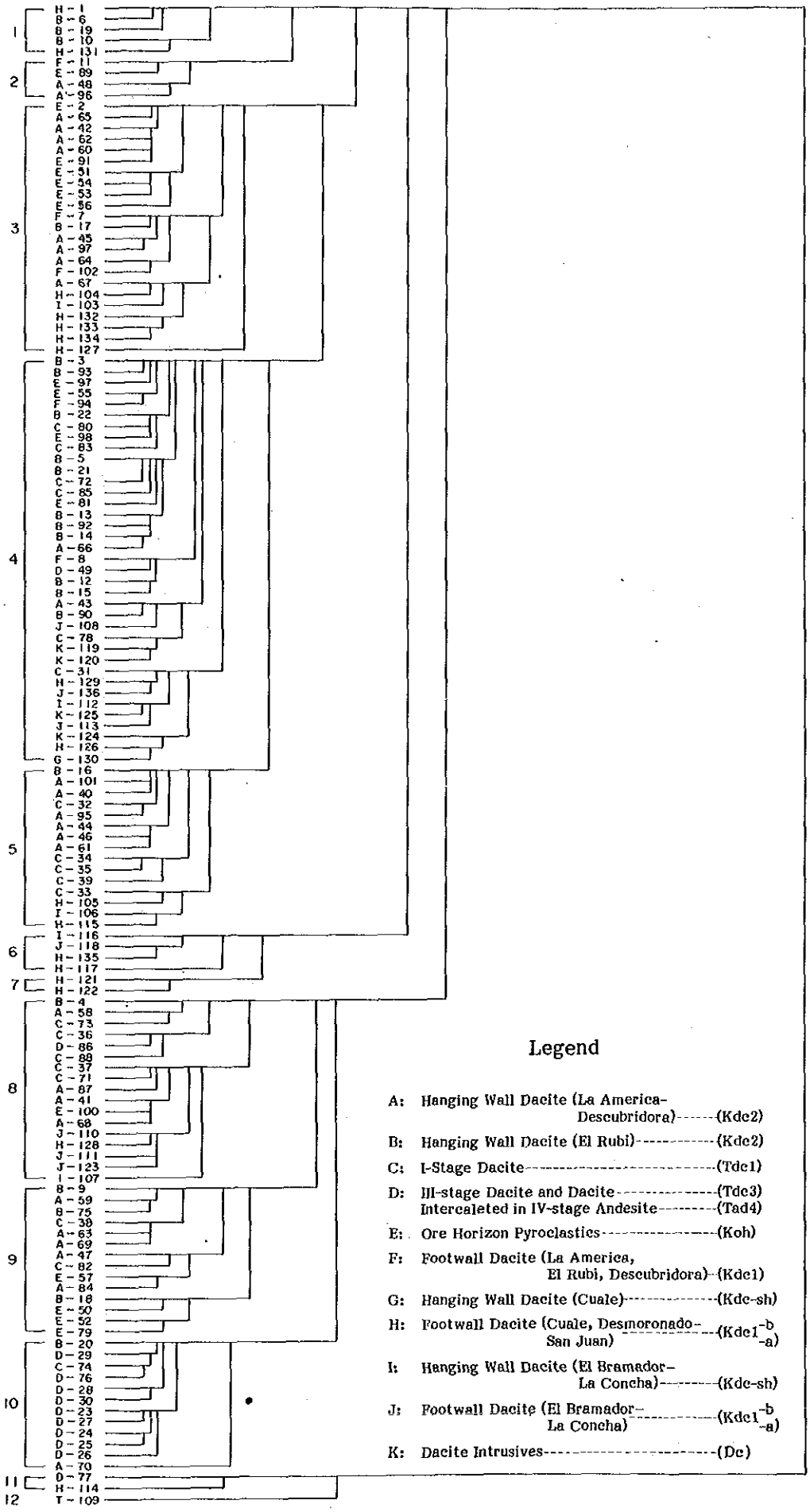

Fig. 4-4 Cluster Dendrogram of Rock Samples

Table 4-8 Average Chemical Composition of Principal Clusters

Composition	Cluster							Average of all rock ●
	3 ○	4 ◇	5 △	6 □	8 ◎	9 ☆	10 +	
SiO_2	76.60	79.49	78.25	76.80	72.41	72.24	75.64	77.67
TiO_2	0.10	0.10	0.11	0.08	0.33	0.20	0.20	0.15
Al_2O_3	11.16	10.26	10.81	9.17	13.22	9.49	12.22	10.41
Fe_2O_3	1.17	0.66	1.01	5.99	1.65	0.99	1.67	1.32
FeO	0.93	0.53	0.30	0.19	0.98	1.67	0.19	0.73
MnO	0.02	0.01	0.01	Tr	0.02	0.07	0.03	0.02
MgO	1.30	0.29	0.24	0.28	0.74	1.59	0.07	0.65
CaO	0.11	0.16	0.02	0.01	0.23	1.75	0.12	0.30
Na_2O	1.58	2.53	0.43	0.05	3.10	2.31	2.48	2.05
K_2O	3.21	4.09	6.26	1.21	3.70	1.51	5.15	3.64
P_2O_5	0.01	0.02	0.02	0.02	0.09	0.04	0.02	0.03
LOI	2.56	0.90	1.70	2.41	2.05	2.76	1.76	1.78
BaO	0.15	0.12	0.14	0.02	0.08	0.18	0.14	0.12

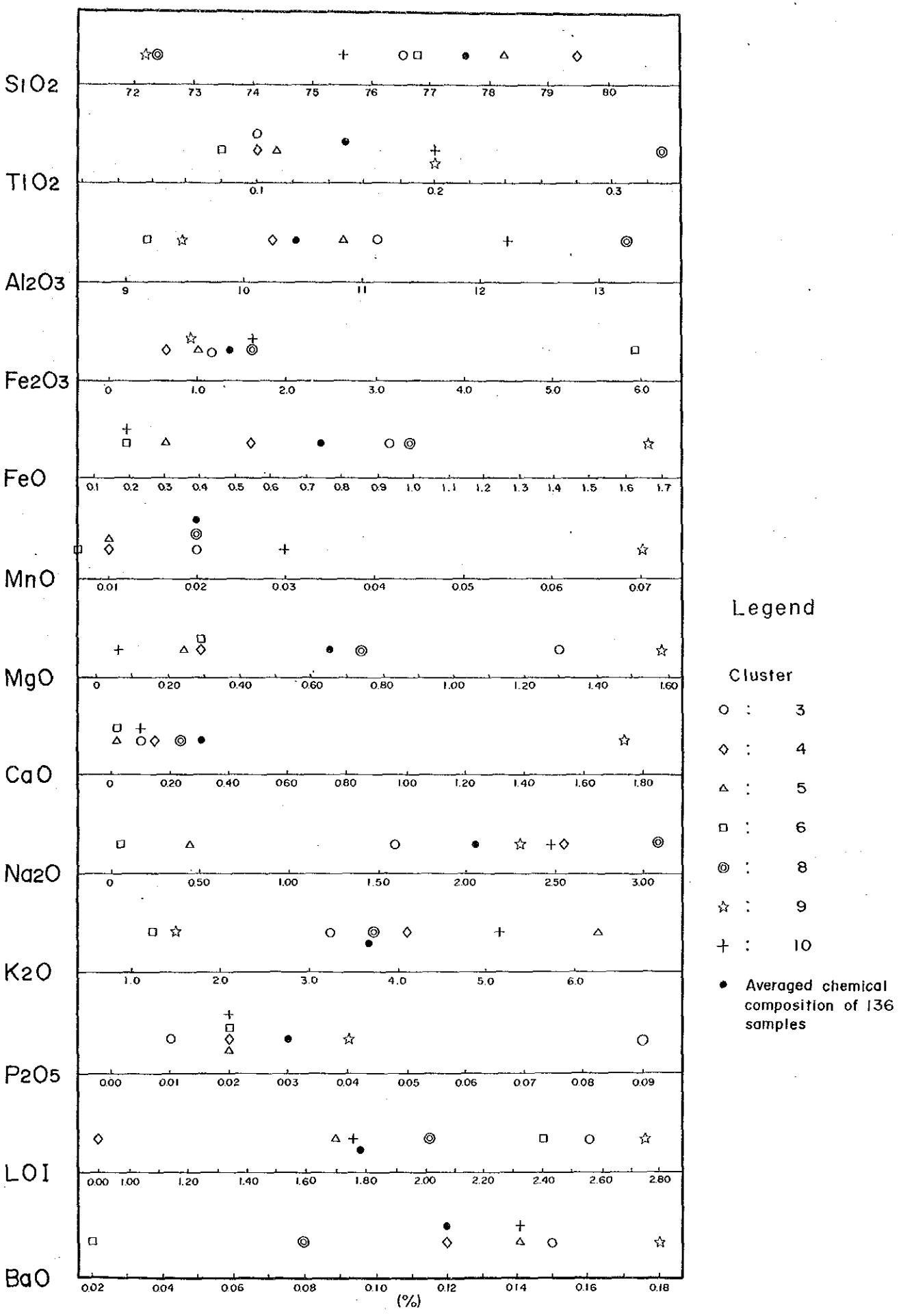

Fig. 4-5 Comparison of Chemical Characteristics of Major Clusters

Cluster 9 and 10 are other principal clusters as shown in Fig. 4-4. No sample from this year's survey area is involved in the clusters. Samples came from the hanging wall dacite (Kdc2) and the ore horizon pyroclastics (koh) in the La America-Descubridora district.

Characteristics of the cluster 9 are poor in SiO_2, rich in MgO and CaO, clearly representing geochemical characters of genuine rocks. Particularly noticeable behaviours of components are not seen in the cluster 10. It means that no mobilized components are involved in the samples and the cluster would be no relation to Kuroko mineralization.

Most of the samples are of the III-stage dacite (Tdc3) of Tertiary System.

As a result of the cluster analysis, it is clarified that each cluster is subjected to alteration, overlapping to their genuine lithogeochemical characters.

In other words, it is possible to classify types of alteration for rocks by cluster analysis.

In summary, it is concluded that cluster 5 is of relating to Kuroko type mineralization, consisting of expected components in Kuroko mineralization-alteration zone.

CHAPTER 5 GEOPHYSICAL SURVEY

CHAPTER 5 GEOPHYSICAL SURVEY

5-1 Survey Method

5-1-1 Measuring Method

The CSAMT (Controlled-Source Audio Frequency Magnetotellurics) survey determines the underground resistivity distribution by transmitting audio frequency current through the grounded dipole, and measurs the electric field (E), parallel to the transmitter dipole, and the magnetic field (H), perpendicular to the electric field.

The CSAMT measurement system (transmitter system and receiver system) is shown in Fig. 5-1. The transmitted current frequencies were 2048, 1024, 512, 256, 128, 64, 32, 16, 8 and 4 Hz (ten in total).

Signals from both electric and magnetic fields are processed by a GDP-12 receiver, which outputs the following:

(1) Apparent resistivity (ρ_a)

(2) Phase difference between electric and magnetic fields (PD)

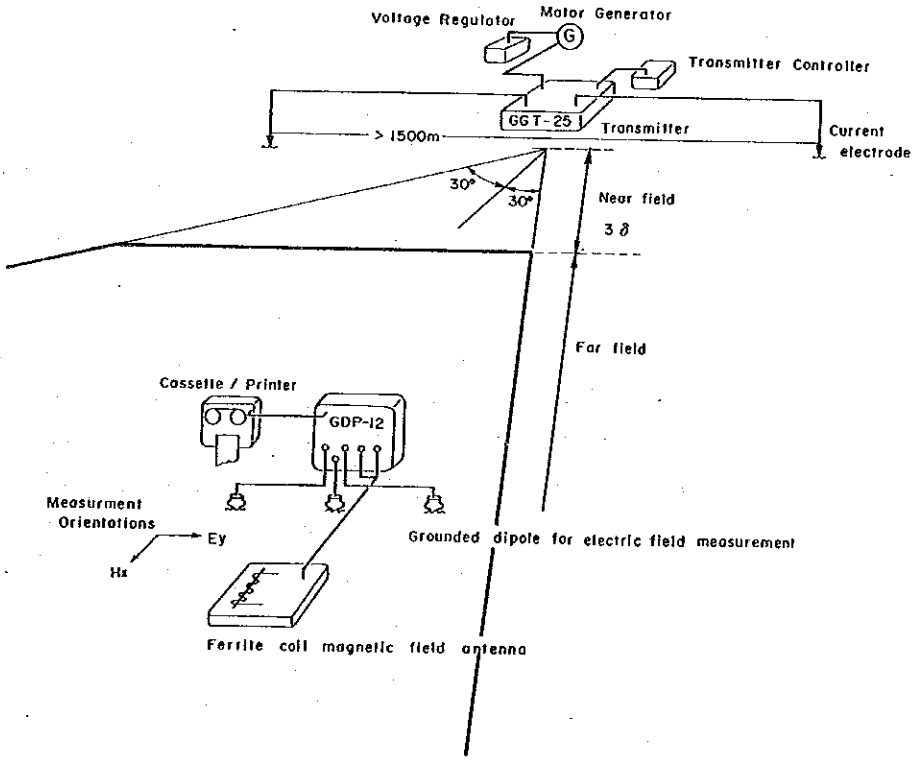

Fig. 5-1 Logistics of CSAMT Survey

As shown in Fig. 5-1, the distance between the transmitter system and the receiver system should be three times or more of the skin depth, and then at the receiving point an assumption of plane electromagnetic waves is considered to be approximately valid (3δ: usually 4 to 8 km).

The skin depth is given by the following equation.

$$\delta = 503\sqrt{\frac{\rho}{f}} \qquad (5\text{-}1)$$

where δ : skin depth (m)
ρ : resistivity ($\Omega \cdot$m)
f : frequency

Using equation (5-1), the relationship between skin depth, and frequency or resistivity for a half space is shown in Table 5-1. As clearly shown in table 5-1, skin depth increases with lower frequencies and higher resistivity. Consequently, the higher resistivity has stronger effect of near field, thus the range of near field data shifts from the lower frequency side to the higher frequency side.

Table 5-1 SKIN DPETH (in Meter)

Remark: Skin Depth (m) = $503 \times \sqrt{\rho/f}$

RESISTIVITY($\Omega \cdot m$) ⟶

FREQUENCY(Hz) ↑

fHz	5	10	20	40	80	160	320	640	1,280	2,560	fHz
2,048	25	35	50	70	99	141	199	281	398	562	2,048
1,024	35	50	70	99	141	199	281	398	562	795	1,024
512	50	70	99	141	199	281	398	562	795	1,124	512
256	70	99	141	199	281	398	562	795	1,124	1,591	256
128	99	141	199	281	398	562	795	1,124	1,591	2,249	128
64	141	199	281	398	562	795	1,124	1,591	2,249	3,181	64
32	199	281	398	562	795	1,124	1,591	2,249	3,181	4,499	32
16	281	398	562	795	1,124	1,591	2,249	3,181	4,499	6,362	16
8	398	562	795	1,124	1,591	2,249	3,181	4,499	6,362	8,998	8
4	562	795	1,124	1,591	2,249	3,181	4,499	6,362	8,998	12,725	4

Since the survey area generally shows higher resistivity, causing much near field effect, the current electrode systems was kept more than 7 km away from the measuring area.

As shown in Fig. 5-2, transmitter dipole No.1 and No.2 were set to the west of the survey area.

The co-ordinates of the electrode systems and so on are shown in Table 5-2.

Table 5-2 Data of Transmitter Dipole

	No. 1		No. 2	
Coordinates	X	Y	X	Y
	-23,275 -23,200	9,550 7,650	-16,463 -16,088	9,200 7,400
Transmitter dipole length	1,900 m		1,850 m	
Directions to the True north	N 2.4° W		N 11.6° W	
Magnetic north	N 12.4° W		N 21.6° W	
Contact Resistance	140 Ω		30 Ω	
Transmitted current	1.5 ~ 4.7 A		3.6 ~ 12.2 A	
Corresponding survey stations	1 ~ 201		133, 202 ~ 318	
Numbers of survey stations	201		118	

Many iron lods were used as current electrodes, so that the total resistance of the current electrode system was decreased as less as possible. In addition, to improve S/N ratio, transmitting current ranging was on 1.5 to 12.2 A and an output range of less than 9.0 kW (max.) was obtained.

Measurement was made at receiving points located more than 60 meters away from conductive objects such as automobiles, and more than 100 meters away from power lines to avoid their interference. To measure electric field, three copper-copper sulphate electrodes were grounded in parallel to the transmitter dipole and 25 meters away each other. On the other hand, to measure magnetic field, a high sensitivity ferrite coil antenna was set more than 9 meters away from the center of the electric field dipole, and perpendicular to the direction of the dipole (potential electrodes).

Fig. 5-3 shows an example log-resistivity vs. log-frequency plot which shows frequency on X-axis and apparent resistivity on Y-axis logarithmically both.

To study the correlations between the results of CSAMT survey and geology, 30 rock and ore samples in total, which represent geology in the survey area, were collected. After all these samples had been formed into nearly rectangular prisms, their resistivity was measured in a wet state by the measurement system shown in Fig. 5-4. The values of resistivity were calculated by the following equation:

$$\rho = (V/I) \cdot (S/1) \quad \text{..... (5-2)}$$

EL ANCA

CABREL

EL NOGAL

LOS CABALLOS DE CABRELO

LOS TECOMATES

LA JOYA

LA VAINILLA

LA HIGUERITA

LAS MOSTAZAS

105°10'00"

105°05'

105°00'

X-20,000

X-15,000

X-10,000

X-5,000

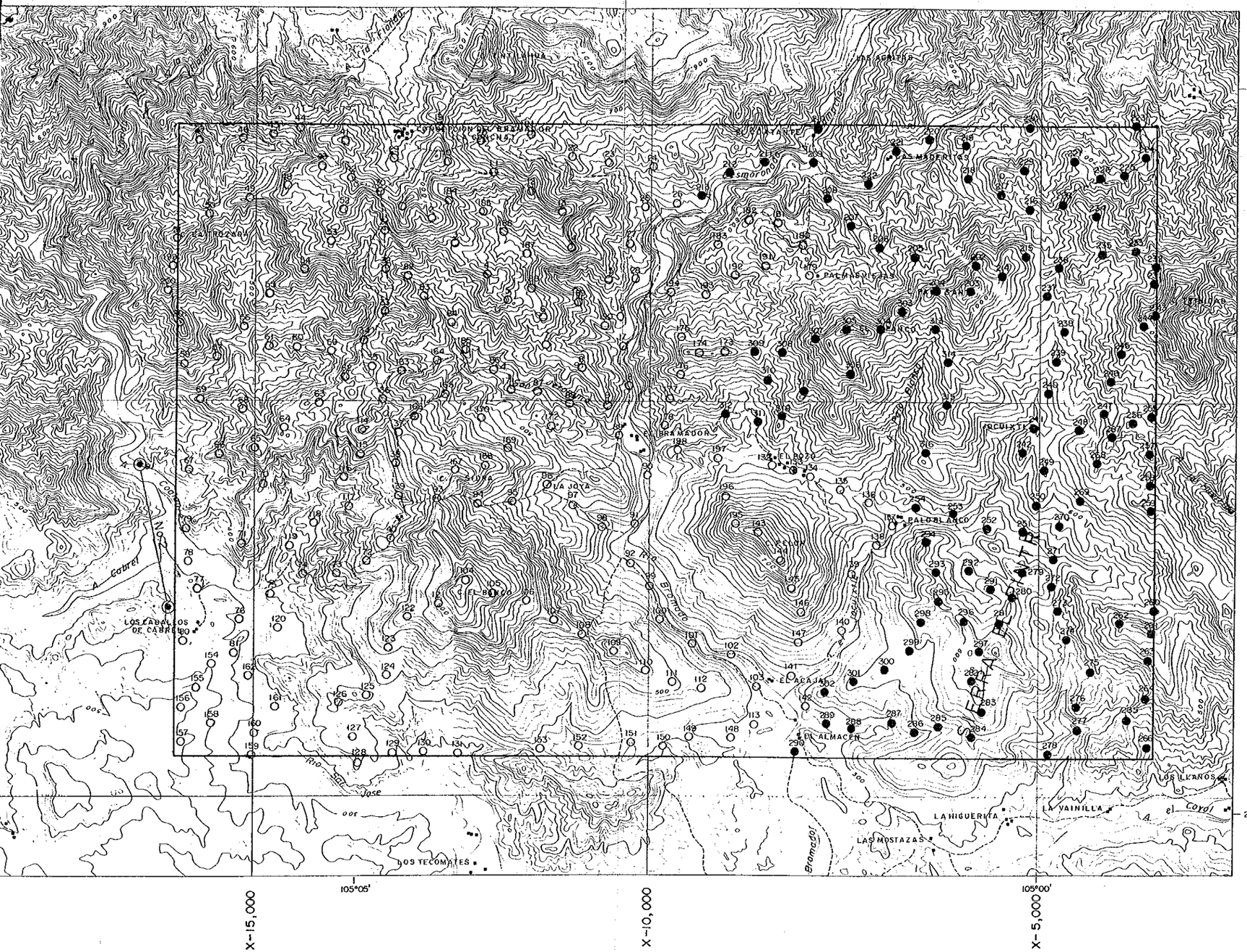

Fig. 5-2 Location Map of CSAMT Survey Stations

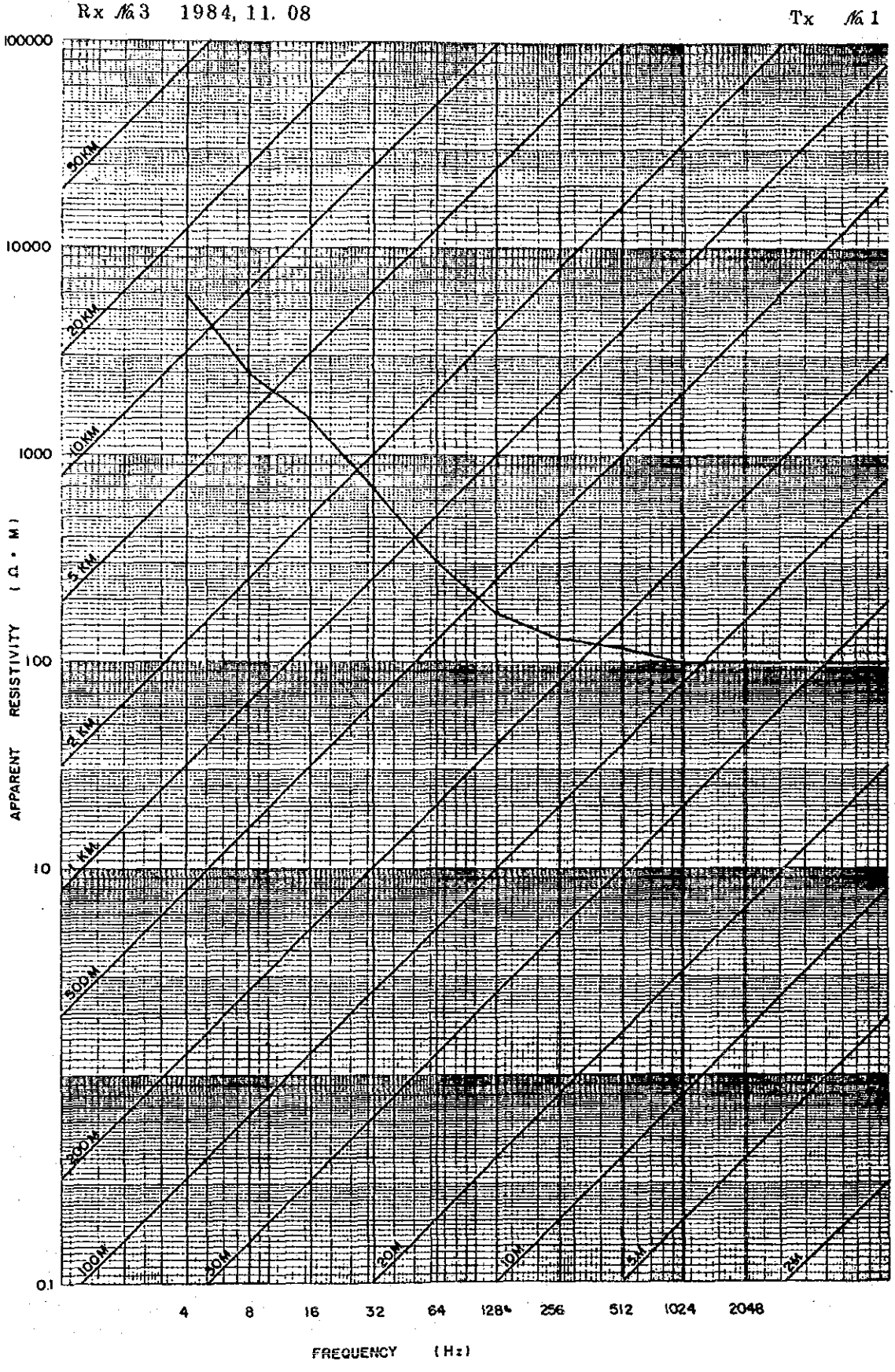

Fig. 5-3 Log-Resistivity versus Log-Frequency Plot

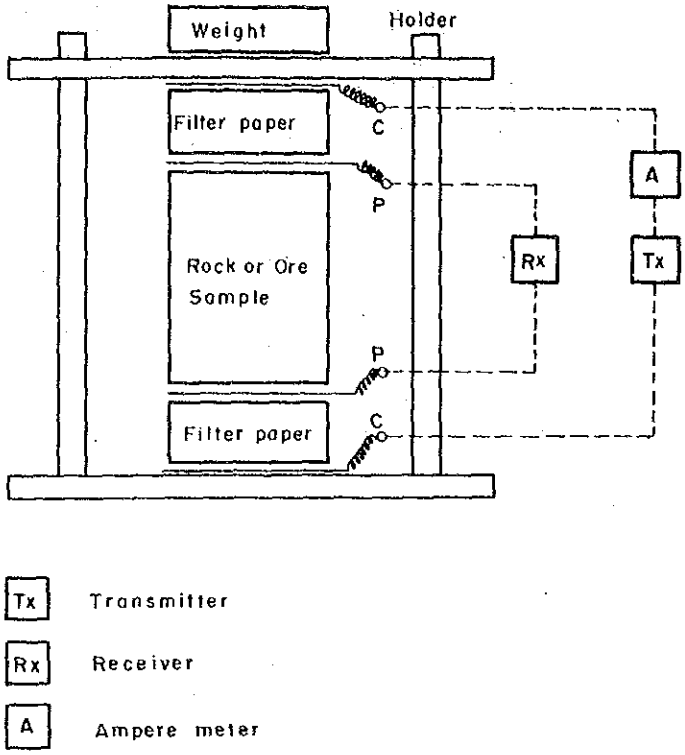

Fig. 5-4 Block Diagram of Laboratory Measurement of Resistivity

where ρ : resistivity ($\Omega \cdot m$)
V : potential difference (V)
I : current (A)
S : cross-sectional area (m^2)
1 : length (m)

5-1-2 Instruments Used

Table 5-3 shows equipment, tools and materials which were used in measurement.

5-2 Deta Processing and Analysis

5-2-1 Data Processing

The intensity and absolute phases of electric and magnetic fields are measured by the GDP-12 receiver, potential dipole and coil antenna, and then the apparent resistivity and the phase difference between the electric and magnetic fields calculated by the microprocessor in the receiver are displayed.

Table 5-3 CSAMT Survey Instruments

System	Equipment	Specification	Number
Transmitter System	Zonge, Inc. Model GGT-25 Transmitter	Output Voltage: 400 V - 800 V Output Current: 0.2 A - 25 A (9.0 kW) Output Ware Form: Rectangular Output Current Frequency: 1/1,024 Hz ~ 2,048 Hz Weight: 113 kg	1
	Zonge, Inc. Model XMT-12 Transmitter Controller	Controle Current Frequency: 1/1,024 Hz ~ 2,048 Hz Weight: 5.8 kg Power Source: 12 V Battery	1
	Zonge, Inc. Model VR-1 Voltage Regulator	Weight: 3.7 kg	1
	Model ZMG-10 Engine-Generator	Maximum output Power: 10 kW Frequency: 400 Hz Rating Voltage: 115 V Engine: 23 Hp, 2 Cylinder, Aircooling	1
Receiver System	Zonge, Inc. Model GDP-12 Receiver	Input Signal: 2 channels AMT Receiving Frequency: 0.5 Hz ~ 2,048 Hz Receiving Voltage Sensitivity: 0.2μV Weight: 15 kg Power Source: 12 V Battery	1
	Zonge, Inc. Model CAP-12 Mini Casset Recorder	Weight: 6.2 kg Power Source: 12 V Battery	1
	Tektronics Model 212 Oscilloscope	Input Signal: 2 channels Power Source: 12 V Battery	1
	Zonge, Inc. AMT Antenna	Weight: 9.8 kg Power Source: 9 V Battery	1
Electrode	Current Electrode Potential Electrode	Iron Rod: ϕ16 mm, Length 80 cm Saturated Copper Sulphate Solution Non-Polarized Electrode	200 10
Wire	Fujikura Electric Kyosan Electric	VSF x 1.25 mm^2 Vinyl Wire CVV_1 x 3.5 mm^2 Vinyl Wire	1000 m 6000 m
Sample Measurement System	Chiba Electronics Institute Model CH-8108A IP Transmitter	Output Current: 1μA ~ 20 mA Output Wave From: Rectangular Output Current Frequency: 0.3 Hz, 3 Hz	1
	Chiba Electronics Institute Model CH-8104R IP Receiver	Receiving Voltage: 1 mV ~ 10 V	1
	Platinum Electrode	Platinum Wire Diameter: 0.3 mm	4
Communication System	Mitsubishi Electric MT-370F05	Transmitting power: 5W Communication Frequency: 903,0375 ~ 904,9875 MHz	4

Next, all data used in measurement and calculation, and the results of calculation are printed by the CAP-12 casette printer. To calculate apparent resistivity, the following Cagniard's equation (1953) being used in the ordinary MT method, is used.

$$\rho a = \left| Ex/Hy \right|^2 (2\pi f \mu) \quad \text{..... (5-3)}$$

where Ex : electric field (V/m), Hy = magnetic field (A·Turn/m)
f : frequency (Hz), μ : permeability in vacuum
$(4 \times 10^{-7}$ H/m)

Hence, equation (5-3) becomes as follows:

$$\rho a = 1.267 \times 10^5/f \cdot \left| Ex/Hy \right|^2 \quad \text{..... (5-4)}$$

For measuring units, (mV/km) and (Gamma) were used for electric and magnetic fields respectively. Therefore, the following equation (5-5) was used to calculate apparent resistivity.

$$\rho a = 0.2/f \cdot \left| Ex/Hy \right|^2 \quad \text{..... (5-5)}$$

In the Measured Data Lists attached to Apx. 10, mean values of E, H, RHO and PD for each frequency are listed. With these values of RHO, a plan of apparent resistivity was drawn for each frequency.

For apparent resistivity pseudo-sections, the following six sections were selected: A-A', B-B', C-C', D-D', E-E' and F-F'. In this case they pass through major apparent resistivity anomalies, and A-A', B-B' and C-C' sections run nearly parallel to the geological structure of this area, while D-D', E-E' and F-F' cross their direction nearly at right angles.

In sections, apparent resistivity values on survey stations near sectional lines were plotted in a high to low frequency in order to draw contour lines as drawn in the plan of apparent resistivity. Apparent resistivity values show the mean resistivity values down to skin depths. Since skin depth is a function of apparent resistivity and frequency as shown in equation (5-1), frequency (Y-axis) does not correspond skin depth directly. These apparent resistivity pseudo-sections show the outline of vertical resistivity distribution underground.

5-2-2 Analytical Method

A simulation technique, curve-matching method, was used for analysis. In this technique, measured values are plotted on the display of a personal computer, and then a log-resistivity vs. log-frequency plot calculated for an arbitrary, resistivity multi-layered model is superposed on the display. Next, this model is corrected so that it approximates the actual CSAMT curves drawn from measured values. An example is shown in Fig. 5-5.

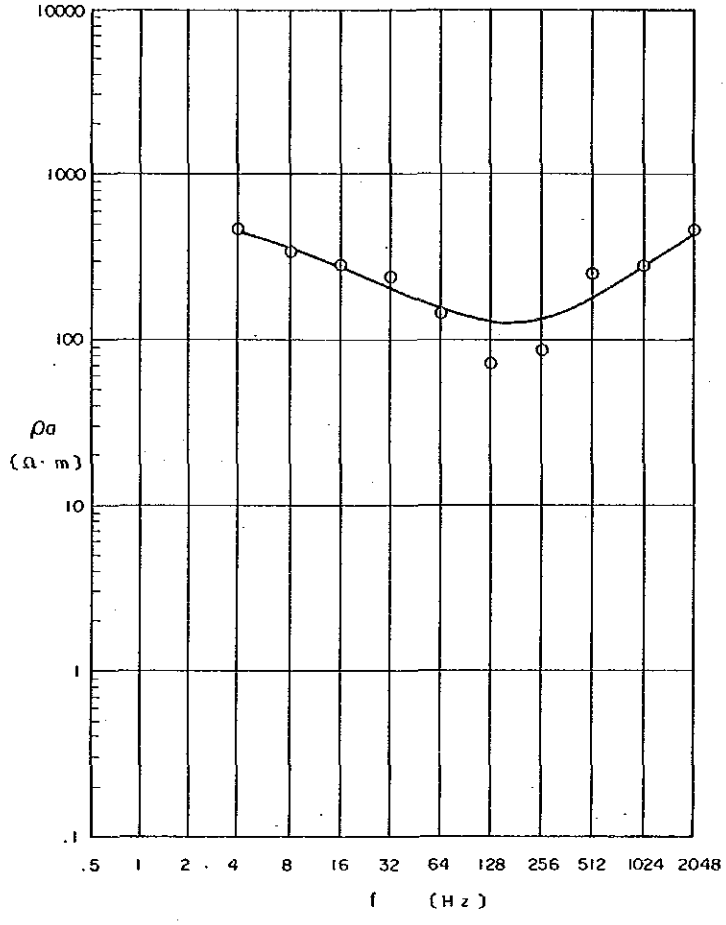

STATION NO. 1

FREQ (Hz)	APPARENT RESISTIVITY OBSERVED (Ω · m)	CALCULATED
2048	463.14	435.06
1024	274.38	282.81
512	246.41	179.68
256	87.31	131.32
128	73.24	124.87
64	142.75	149.82
32	236.31	199.93
16	231.60	269.57
8	334.79	351.14
4	460.95	435.51

CSAMT LAYERED MODEL

	RESISTIVITY (Ω · m)	DEPTH (m)
ρ I	600.00	
		150.00
ρ II	50.00	
		300.00
ρ III	800.00	

Fig. 5-5 Log-Resistivity versus Log-Frequency Plot with Calculated Curve

The resistivity calculation method for layered model used for the above simulation is as follows:

The surface impedance (Z(0)) of the (n+1) the layers, for a layered structure with resistivity values of respective layers ρ_1, ρ_2, ..., ρ_n, ρ_{n+1} and depth of respective layers Z_1, Z_2, ..., Z_n is shown by the following equation.

$$Z(o) = \frac{Ex}{Hy}\Big|_{z=o} = \frac{i\omega\ (A_0 + B_0)}{\theta o\ (A_0 - B_0)} \qquad \text{..... (5-6)}$$

where

$$A_0 + B_0 = A_1 + B_1$$
$$\theta_0\ (A_0 - B_0) = \theta_1\ (A_1 - B_1) \qquad \text{..... (5-7)}$$

$$\left.\begin{aligned} &A_j \exp(-\theta_j Z_j) + B_j \exp(\theta_j Z_j) \\ &\quad = A_{j+1} \exp(-\theta_{j+1} Z_j) + B_{j+1} \exp(\theta_{j+1} Z_j) \\ &\theta_j \left[A_j \exp(-\theta_j Z_j) - B_j \exp(\theta_j Z_j) \right] \\ &\quad = \theta_{j+1} \left[A_{j+1} \exp(-\theta_{j+1} Z_j) - B_{j+1} \exp(\theta_{j+1} Z_j) \right] \end{aligned}\right\} \text{..... (5-8)}$$

$$(j = 1, 2, \ldots\ldots n)$$

$$\left.\begin{aligned} A_n &= \frac{\theta_{n+1} + \theta_n}{2\theta_n} \exp\left[-(\theta_{n+1} - \theta_n)\ Z_n \right] \\ B_n &= \frac{\theta_{n+1} - \theta_n}{2\theta_n} \exp\left[-(\theta_{n+1} - \theta_n)\ Z_n \right] \end{aligned}\right\} \text{..... (5-9)}$$

Where the CGS-emu unit system is used and θ shows the number of waves.

$$\theta_j = \left(\frac{4\pi i\omega}{\rho_j}\right)^{1/2} \qquad (j = 1, 2, \ldots\ldots n)$$
$$\omega = 2\pi f$$

On the one hand, since 1 mV/km = 1 emu, 1 $\Omega \cdot$m = 10^{11} emu, and 1 γ = 10^{-5} emu, the apparent resistivity equation (5-5) can be represented in the CGS-emu unit system as follows:

$$\rho_a = \frac{2}{f}\left|Z(0)\right|^2 \quad \text{(emu)} \qquad \text{..... (5-10)}$$

Accordingly, apparent resistivity (ρa) can be determined from equations (5-6) to (5-10), and the equation for calculating ρa in $\Omega \cdot$m unit becomes as follows:

$$\rho_a = 2/f \cdot |Z_{(0)}|^2 / 10^{11} \quad (\Omega \cdot m) \quad \text{..... (5-11)}$$

In consideration of the resistivity layered model, results obtained from Bostic Inversion were referred to.

The log-resistivity versus log-frequency plots frequently show three zones, far field (F), transition zone (T) and near field (N) as seen in Fig. 5-6. Near field data shows a straight line with approximately -45° gradient on the low frequency side of log-resistivity versus log-frequency Plot.

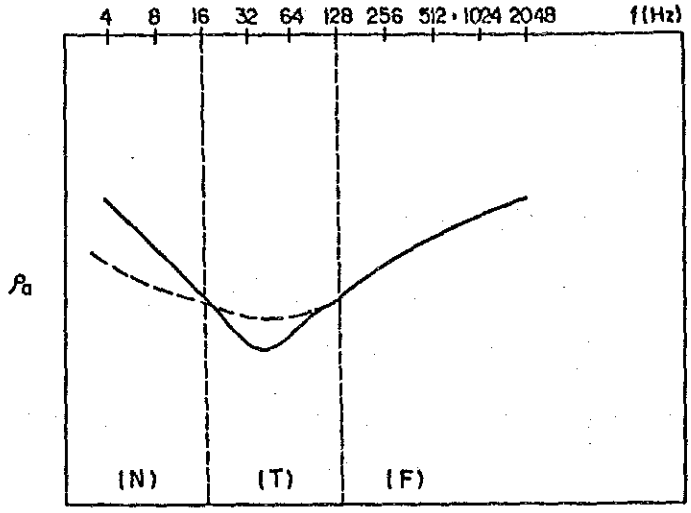

Fig. 5-6 Typical CSAMT Log-Resistivity versus Log-Frequency Plot

(F) : far field data
(T) : transition zone
(N) : near field data

The dashed line gives the Calculated Curve

(Zonge Inc., Interpretation Guide for CSAMT Data, 1982)

For reference the features of log-resistivity versus log-frequency plots of the two-layered structure model are shown in Fig. 5-7. In the figure, the curves show transition zones as well as near field zones when the second layer is of high resistivity.

Thus, in this analysis, a model having high resistivity at the lowest layer was assumed for simulation of data including near field and transition zones. In addition, curve matching was carried out so that calculated curves passed the upper part of transition zones and lower part of near field zones as shown in Fig. 5-6.

Various plans of resistivity structure were produced based on the layered resistivity model for each survey station obtained from simulation. These plans show the underground resistivity structure at the depths of 100 m, 200 m, 400 m and 600m below the surface of each survey station, and 200 m, 400 m above the sea level.

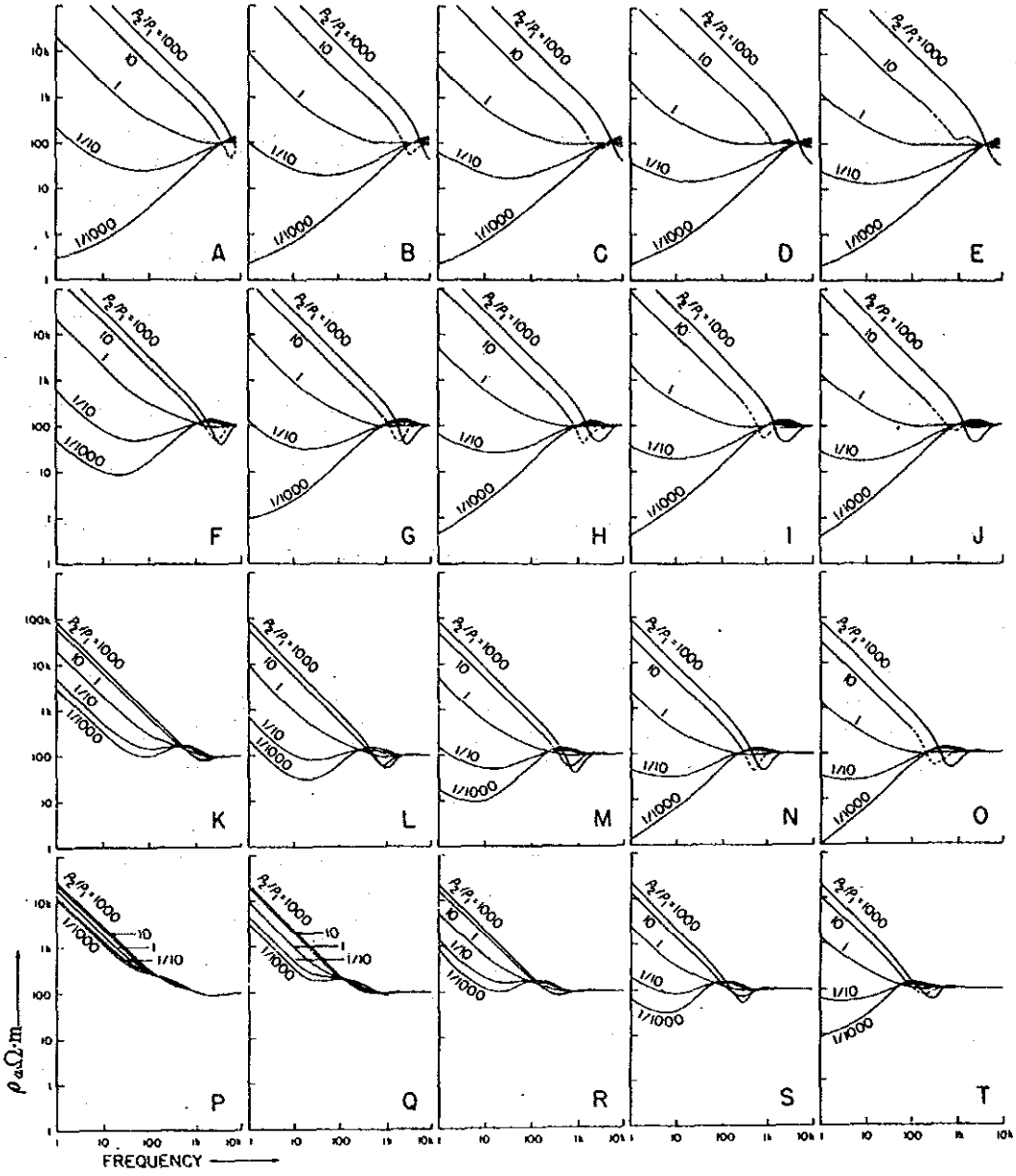

D	R = 5 0 0 *m*	7 5 0 *m*	1, 0 0 0 *m*	1, 5 0 0 *m*	2, 0 0 0 *m*
5 0 *m*	A	B	C	D	E
1 2 5 *m*	F	G	H	I	J
2 5 0 *m*	K	L	M	N	O
5 0 0 *m*	P	Q	R	S	T

Fig. 5-7 Representative Families of Curves for Various Depth to the Bottom of the First Layer and Various Ranges

ρ_1, ρ_2: resistivity of the first and second layers respectively.
$\rho_1 = 100\ \Omega \cdot m$
R: distance between Tx dipole and receiver point
D: thickness of the first layer

(Goldstein & Strangway, 1975)